ions (Dhara, 1970). In this study we exploited this character of CDDP3, to establish an efficient procedure of CDDP encapsulation into liposomes at a high concentration.

As for the precedent targeting delivery of CDDP, cationic liposomes conjugated with 3,5-dipentadecycloxybenzamidine hydrochloride (TRX-20) encapsulating CDDP were shown to be significantly effective to suppress tumor growth and liver metastasis targeting chondroitin sulfate proteoglycans on the malignant cell surface (Lee et al., 2002). Here in this study, we employed a new formula for anionic liposomes conjugated with Sialyl Lewis^X (SLX), which specifically and efficiently targeted E-selectin and accumulated in tumors *in vivo* (Hirai et al., 2007a,b). Liposomes with SLX showed affinity to E-selectin expressed on tumor vascular endothelial cells and exhibited rolling action on the vascular endothelial cells. The SLX-coated liposomes then entered the gaps of the vascular walls, where permeability is augmented by tumor angiogenesis (Bevilacqua et al., 1989; Vestweber and Blanks, 1999; Mayer et al., 1998; Liu and Rabinovich, 2005).

2. Materials and methods

2.1. Materials

CDDP, potassium tetrachloroplatinate (II), potassium iodide, ammonia aqueous solution (28%), silver nitrate, dipalmitoylphosphatidyl choline (DPPC), cholesterol (Chol), dicetylphosphate (DCP), sodium cholatehydrate (cholic acid) human serum albumin (HSA), sodium periodate, deuterium oxide (D_2O) sodium hexachloroplatinate, tris(hydroxymethyl)aminomethane (Tris), DMEM, RPMI-1640, gelatin, fetal bovine serum (FBS) and penicillin–streptomycin solution were purchased from Sigma (St. Louis, MO). Ganglioside was purchased from Avanti Polar Lipids (Alabaster, AL, USA). Dipalmitoylphosphatidylethanolamine (DPPE) was purchased from Alexis (Plymouth Meeting, PA). N-tris(hydroxymethyl)methyl-3-amino-propane sulfonic acid (TAPS) and *n*-(2-hydroxyethyl) piperazine-*n*′-(2-ethanesulfonic) acid were purchased from Dojin Chemical (Kumamoto, Japan). Sodium cyanoborohydrate was purchased from Aldrich (Milwaukee, WI). Sialyl Lewis^X (SLX) was purchased from EMD Chemicals (Gibbstown, NJ). Bis(sulfosuccinimidyl)suberate (BS_3) and 3,3-dithiobis(sulfosuccinimidylpropionate) (DTSSP) were purchased from Pierce Biotechnology (Rockford, IL, USA). Determiner TC555 kit was purchased from Kyowa Medics (Tokyo, Japan). Potassium dichloroplatinum was purchased from Nacalai Tesque (Kyoto, Japan). In situ apoptosis detection kit was purchased from Takara BIO (Kyoto, Japan). TNF-α was purchased from R&D Systems (Minneapolis, MN). FITC labeled anti-mouse IgG antibody was purchased from Santa Cruz (Santa Cruz, CA). Collagen was purchased from Roche (Basel, Switzerland). Female BALB/c mice were purchased from Japan SLC (Shizuoka, Japan). Ehrlich's ascites tumor (EAT) cells were purchased from RIKEN Bio Resource Center (Ibaragi, Japan). Human lung cancer A549 cells and Hybridoma (CCL-3) were obtained from the ATCC (Manassas, VA). Human umbilical vein endothelial cells (HUVEC) and human endothelial cell medium were purchased from DS Pharma Biomedical (Osaka, Japan).

2.2. Preparation of CDDP3

CDDP3 was synthesized by the method of Dhara (1970). Briefly, potassium tetrachloroplatinate (II) (4.15 g, 10 mmol) was dissolved in distilled water. Potassium iodide (6.64 g, 40 mmol) was then added and stirred on ice for 5 min under a nitrogen atmosphere and light shielding. Ammonia aqueous solution (28%, 1.35 mL) was added to this reaction solution, and stirred on ice for 3 h. The yellow crystals formed were washed with distilled water and ethanol, and dried at 40 °C for 10 h under decompression. At this stage, 4.49 g of *cis*-diammineiodeplatinum (II) (CDDP2) was obtained. CDDP2 (2.41 g, 5 mmol) was suspended in distilled water. Silver nitrate (1.68 g, 9.9 mmol) was then added and stirred on ice for 24 h under light shielding. The reaction solution was passed through a paper filter to remove any silver iodide. The filtrate was then concentrated using a rotating evaporator and white crystals were obtained. These crystals were washed with iced distilled water and ethanol, and then dried at 40 °C for 10 h under decompression. The final yield of CDDP3 was 1.0 g.

2.3. Measurement of absorption spectrum

The absorption spectra were measured using a UV spectrophotometer (Model UV-2500PC, Shimazu, Japan) at 5, 10, 15, 30, 60, 120 and 180 min after dissolving 5 mg of CDDP3 in 1 mL of 150 mM NaCl. In contrast, 2 mg of CDDP was dissolved in 1 mL of 150 mM NaCl and 24 h after dissolution, the absorption spectrum was measured. The absorption spectrum of 150 mM NaCl was deducted from each absorption spectrum.

2.4. Preparation of CDDP-encapsulated liposomes

The liposomes were prepared using an improved cholate dialysis method (Yamazaki, 1989; Yamazaki et al., 1994). DPPC, Chol, ganglioside, DCP and DPPE were mixed at the molar ratio 35:40:5:15:5 (total lipid 456 mg) and then cholic acid (469 mg) was added to facilitate micelle formation. The mixture was dissolved in 30 mL of methanol/chloroform (1:1, v/v) solution. The solvent was evaporated using a rotating evaporator at 37 °C to produce a lipid film, which was dried under vacuum. This lipid film was dissolved in 30 mL of 10 mM TAPS buffer without NaCl at pH 8.4, followed by sonication to obtain a suspension of uniform micelles. One gram of CDDP3 was completely dissolved in 70 mL of 10 mM TAPS (pH 8.4), without NaCl and the pH was readjusted to 8.4 with 1 M NaOH. The CDDP3 solution was then added to the micelle suspension described above. To subsequently remove cholic acid and free CDDP3, the micelle solution was ultrafiltrated with 10 mM TAPS (pH 8.4) using an ultrafiltration cell holder (Amicon model 8200, Millipore, Billerica, MA) fitted with an ultrafiltration disc membrane (molecular cut off 10,000) (Amicon PM10, Millipore, Billerica, MA). One hundred milliliter of the liposome encapsulated CDDP3 was obtained. To convert CDDP3 in the liposomes into CDDP, the buffer was exchanged to 10 mM TAPS, pH 8.4, containing 150 mM NaCl by ultrafiltration through an ultrafiltration disc membrane (molecular cut off: 300,000) (Amicon XM300, Millipore, Billerica, MA). Hydrophilization treatment and SLX conjugation on the surface of liposomes were carried out as described previously (Hirai et al., 2007a). To exchange buffer, the solution was ultrafiltrated with sodium 5 mM hydrogencarbonate buffer (CBS, pH 8.5) through Amicon XM300 membrane. One hundred milligram of the crosslinking agent BS_3 was added to 100 mL of the liposome solution, and stirred at 25 °C for 2 h. The suspension was then further stirred overnight at 4 °C after which BS_3 was conjugated to the liposome surface. Four hundred milligram of Tris was then added, and stirred at 25 °C for 2 h and further stirred overnight at 4 °C to bind Tris to BS_3. The suspension was ultrafiltrated with 10 mM TAPS (pH 8.4) through an Amicon XM300 membrane to remove any residual Tris. Human serum albumin (HSA) was coupled to the liposome surface as previously described (Yamazaki, 1989; Yamazaki et al., 1994). To oxidize the liposome surface, 108 mg of sodium periodate was added to 100 mL of the liposome solution and stirred at 4 °C overnight. To remove residual sodium periodate, the suspension was ultrafiltrated with 10 mM phosphate saline buffer (PBS, pH 8.0) through an Amicon XM300 membrane. Two hundred mil-

ligram of HSA was then added to the suspension and stirred at 25 °C for 2 h. Then 31.3 mg of sodium cyanoborohydrate was added, and stirred at 25 °C for 2 h and further overnight at 4 °C. To remove any residual sodium cyanoborohydrate, the solution was ultrafiltered with CBS buffer (pH 8.5) through an Amicon XM300 membrane. SLX was conjugated to the liposome surface through DTSSP. One hundred milligram of DTSSP, a crosslinking agent, was added to 100 mL of liposomes solution, and stirred at 25 °C for 2 h, and further overnight at 4 °C. To remove residual DTSSP, the solution was ultrafiltrated with CBS buffer (pH 8.5) through an Amicon XM300 membrane. The amination of the reducing group terminal of SLX was accomplished through the glycosyl amination reaction. Eight milligram of SLX was dissolved in 2 mL of distilled water. One gram of ammonium hydrogencarbonate was added and stirred at 37 °C for 3 days. Aminated SLX was added to reach a final concentration of 50 μg/mL and stirred at 25 °C for 2 h. Tris was then added to a final concentration of 132 mg/mL, and stirred overnight at 4 °C for repeated hydrophilization of the liposome surface. To remove any residual SLX and Tris, the solution was ultrafiltrated with 20 mM HEPES (pH 7.2) through an Amicon XM300 membrane. The preparation of liposomes without SLX was similar to the CDDP-SLX-Lip case except for the process for binding SLX. In the studies using animals, CDDP-Lip and CDDP-SLX-Lip were further concentrated 20-fold by ultrafiltration with 20 mM HEPES buffer (pH 7.2) using an Amicon XM300 membrane.

2.5. Physiochemical characterization of CDDP-SLX-Lip

Average particle size and zeta-potential of liposomes that were prepared in water were determined by dynamic light scattering spectrophotometry (Zetasizer Nano-S90, Malvern, Worcestershire, UK) at 25 °C. The instrument was calibrated with standard latex nanoparticles (Malvern, Worcestershire, UK). Experimental values were the average of three different formulations.

2.6. Analysis of lipid concentration

Lipid concentrations of CDDP-Lip and CDDP-SLX-Lip were measured as total cholesterol in the presence of 0.5% TritonX-100 using a Determiner TC555 kit. The lipid concentration was calculated from the molar ratio of each lipid (4.5) by the following formula (Eq. (1)):

$$\text{lipid concentration (mg/mL)} = \text{cholesterol concentration (mg/mL)} \times 4.5 \quad (1)$$

2.7. Measurement of CDDP, calculation of CDDP concentration and definition of encapsulation efficiency and loading efficiency

CDDP-SLX-Lip were diluted to 10,000-fold with distilled water and the concentration of platinum was measured using automatic a flameless atomic absorption spectrophotometer (FAAS) (Model AA-6700, Shimadzu, Kyoto, Japan). Potassium dichloroplatinate was used as a standard. A calibration curve with platinum concentrations in the range of 50–250 ng/mL was run before analysis of each sample type. The amounts of CDDP were calculated by the following formula (Eq. (2)):

$$\text{CDDP concentration} = A \times \frac{300}{195} \quad (2)$$

where A is the concentration of platinum, 300 is the molecular weight of CDDP, and 195 is the molecular weight of platinum. "Encapsulation efficiency" and "loading efficiency" were defined by the following formula Eqs. (3) and (4), respectively.

$$\text{encapsulation efficiency (\%)} = \frac{\text{amount of CDDP in liposomes}}{\text{initial amount of CDDP}} \times 100 \quad (3)$$

$$\text{loading efficiency} = \frac{\text{CDDP concentration (mg/mL)}}{\text{lipid concentration (mg/mL)}} \quad (4)$$

Namely, "CDDP to lipid weight ratio" was defined as "CDDP loading efficiency".

2.8. ^{195}Pt NMR analysis

CDDP-SLX-Lip were concentrated by ultrafiltration using an Amicon XM300 membrane, and suspended in D_2O to a final platinum concentration of 137 mM. CDDP and CDDP3 were dissolved in D_2O to final concentrations of 6.6 and 137 mM, respectively. Sodium hexachloroplatinate was dissolved in D_2O to a final concentration of 50 mM as the external standard liquid. Each sample was put into 5-mm-width NMR sample tubes (GL Sciences, Tokyo, Japan) and ^{195}Pt NMR spectra were measured at 25 °C using NMR system (Model INOVA-600, Varian, Palo Alto, CA, USA).

2.9. Evaluation of CDDP leakage from CDDP-SLX-Lip

CDDP-SLX-Lip were stored in 20 mM HEPES buffer (pH 7.2) at 4 °C for 3 months. To remove any CDDP leakage from CDDP-SLX-Lip, the liposomes solution was ultrafiltrated using an Amicon XM300 membrane. The concentration of platinum incorporated into the liposomes was measured by FAAS and the amount of CDDP was calculated as described above. The CDDP concentration in CDDP-SLX-Lip after storage for 3 months was compared with that of CDDP in the liposomes immediately after preparation.

2.10. Acute toxicity evaluation

CDDP (18 and 25 mg CDDP/kg body weight), CDDP-SLX-Lip (18, 25 and 50 mg CDDP/kg body weight), saline solution and empty liposomes with SLX (lipid: 700 mg/kg body weight) were administered into the tail veins ($n = 4$) of female BALB/c mice (8 weeks) and the survival rate was examined for 14 days after administration. The lipid dose of empty liposomes with SLX was adjusted to the lipid dose in the case of CDDP-SLX-Lip at 50 mg CDDP/kg body weight. The body weight was measured simultaneously as an indicator of systemic toxicity. Body weight was measured for 5 days after administration with electric balance (Model EK-600i, A &D, Tokyo, Japan). Body weight (%) was calculated by the following formula Eq. (5).

$$\text{body weight (\%)} = \frac{\text{body weight at measurement day after injection}}{\text{body weight before injection}} \times 100 \quad (5)$$

The statistical analysis of the body weight change data were carried out by Mann–Whitney U-test.

For histological and histochemical analysis, CDDP or CDDP-SLX-Lip were injected into the tail vein of normal mice with a dose of either 25 mg CDDP/kg body weight. The kidney, spleen and liver were excised at 3 days after administration and fixed in 10% neutral formalin solution. Paraffin-embedded 2 μm-thick sections were stained with hematoxylin and eosin (HE). TUNEL staining was carried out to detect apoptosis with an in situ apoptosis detection kit followed by HE staining.

All the animal experiments throughout this study were conducted in full compliance with local and national ethical and regulatory principles for animal care.

2.11. Cell cultures

EAT cells and A549 cells were cultured in DMEM supplemented with 10% heat-inactivated FBS, 100 U/mL penicillin and 100 μg/mL streptomycin at 37 °C under atmosphere of 5% CO_2/95% air. HUVEC was cultured in medium for HUVEC (KJB-110, DS Pharma, Japan) supplemented with 10% FBS, 100 U/mL penicillin and 100 μg/mL streptomycin at 37 °C under atmosphere of 5% CO_2/95% air.

2.12. Detection of E-selectin on HUVEC

Anti-E-selectin monoclonal antibody was prepared from the ascites fluid of female Balb/c mice (8 weeks), which received CCL-3 hybridoma. Glass slides in 12-well plates were seeded with 1×10^5 HUVEC per well and cells were incubated in 500 μL of medium at 37 °C for 24 h. EAT cells were cultured until 100% confluent. Five hundred microliter of the supernatant culture medium of EAT or the complete medium of EAT was added to 500 μL of the culture medium of HUVEC. TNF-α was added at 10 ng/mL and HUVEC were cultured for 4 h at 37 °C under atmosphere of 5% CO_2/95% air. After 4 h, HUVEC were then fixed with 3.7% formaldehyde in PBS and at room temperature for 15 min and washed twice with PBS and 0.1% TritoX-100 in PBS. 0.1% of BSA in PBS was added to the each well and incubated at room temperature for 20 min. Anti-E-selectin monoclonal antibody was added at 10 μg/mL and incubated at room temperature for 1 h. HUVEC were then washed twice with PBS, stained with 5 μg/mL FITC labeled anti-mouse polyclonal antibody at room temperature for 1 h and washed twice with PBS. For staining cytoskeleton, rhodamine phalloidin was added at 5 U/mL to HUVEC cultures and incubated at room temperature for 20 min and washed twice with PBS and water. The fluorescence of FITC and rhodamine was observed with fluorescent microscope (Model CKX41, Olympus, Tokyo, Japan).

2.13. Detection of E-selectin in vascular vessels of EAT tumor section

EAT cells (5×10^6 cells/mouse) were transplanted subcutaneously in the back of female BALB/C nude mice. After 10 days, tumors were excised and fixed in 10% neutral formalin solution (Wako) for 24 h. After fixation, the tissues were dehydrated, cleared, infiltrated and embedded with paraffin. Then 4 μm-thick sections were cut out for hematoxylin and eosin (HE) staining and for double immunohistochemistry. For immunological staining, sections were deparaffinized and blocked with 10% goat serum containing 3% TritonX-100 for 1 h at room temperature, sections were incubated with anti-E-selectin antibody (10 μg/mL) for 1 h at 37 °C and rinsed three times in PBS for 5 min each. Then sections were further incubated with FITC labeled goat anti-mouse IgG antibody (Santa Cruz) and *lycopersicon esculentum* lectin (LEL) conjugated with Texas red (Vector Labs) for 1 h at room temperature followed by three times of wash with PBS for 5 min. The sections were mounted with glycerol–PBS (9:1) and observed under an Olympus IX81 microscope equipped with a light fluorescence device (Olympus).

2.14. Targeting tumor of CDDP-SLX-Lip

To prepare EAT tumor-bearing mice, 5×10^6 cells were subcutaneously injected into the right femoral region of 6-week-old female BALB/c mice. Ten days after injection, CDDP-SLX-Lip, CDDP-Lip or CDDP were injected into the tail veins at a dose of 2 mg CDDP/kg body weight. At 48 h after administration, the tumors were excised and soaked in 1 mL of 70% HNO_3 per 0.1 g of each tumor tissue followed by incubation in a water-bath at 60 °C for 1 h. After being cooled to room temperature, supernatant was diluted 4-fold with distilled water. To determine the recovery of platinum, blank tumor tissues samples were spiked with 125 ng CDDP for 1 h, followed by digestion with nitric acid and dilution with distilled water. The amount of platinum in the tumor tissues was measured by FAAS and the amounts of CDDP were calculated as described above. The recovery of platinum after incubation of tumor tissues with CDDP was 82–95%. The statistical analysis was carried out by the standard Student's *t*-test.

2.15. In vivo antitumor activity

To prepare A549 tumor-bearing mice, 1×10^7 cells were subcutaneously injected into the right femoral region of 6-week-old female BALB/c mice at 5, 12 and 19 days after injection, CDDP-SLX-Lip, CDDP-Lip or CDDP were injected into the tail veins at a dose of 25 mg CDDP/kg body weight ($n = 4$). Saline solution was injected into control group ($n = 4$). At 5, 12, 19 and 26 days after injection, the length and width of the tumors were measured using digital calipers (Model CD-20C, Mitsutoyo, Japan), and tumor volume was calculated by the following formula (Eq. (6)).

$$\text{volume } (\text{mm}^3) = \text{length} \times \text{width}^2 \times 0.5 \quad (6)$$

The statistical analysis was carried out by the standard Student's *t*-test.

3. Results

3.1. Conversion of CDDP3 to CDDP

CDDP has a structure coordinating chloride ions at the *cis* location (Fig. 1A) while CDDP3 has nitrate ions in place of chloride (Fig. 1B) with solubility in water about 10 times higher than that of

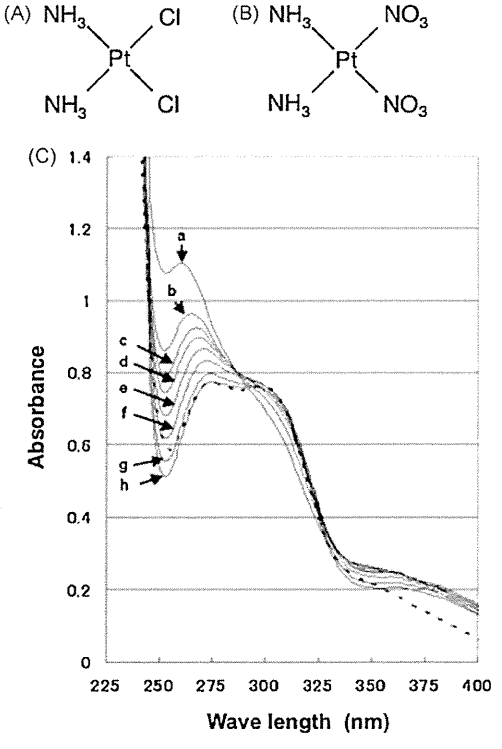

Fig. 1. Conversion from *cis*-diamminedinitratoplatinum (II) (CDDP3) to CDDP. Chemical structures of CDDP (A) and CDDP3 (B). (C) Time-dependent shifts in absorption spectrum of 13.7 mM CDDP3 placed in 150 mM NaCl solution for a, 0; b, 5; c, 10; d, 15; e, 30; f, 60; g, 120; h, 180 min. The dotted line shows the absorption spectrum of 6.6 mM CDDP solution at 24 h after dissolving in 150 mM NaCl solution.

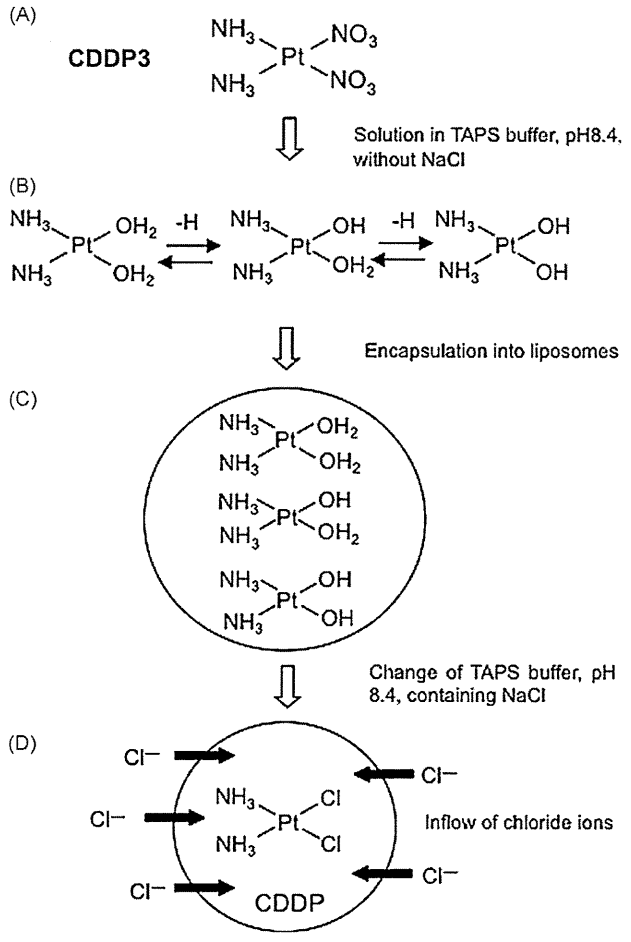

Fig. 2. Scheme of CDDP encapsulation into liposomes using CDDP3. (A) CDDP3 in TAPS, pH 8.4, without NaCl. (B) CDDP3 is in a reversible equilibrium state where H_2O molecules are coordinated due to high solubility of CDDP3 in water. (C) CDDP3 are incorporated in liposomes at this stage, they will show various molecular forms in the liposomes. (D) Change of buffer TAPS, pH 8.4, containing 150 mM NaCl, makes flow of chloride ions into the liposomes and then CDDP is produced by forming coordinate bonds preferentially with chloride ions.

CDDP. The absorption spectra showed that CDDP3 gradually converted to CDDP during incubation in 150 mM NaCl for 24 h (Fig. 1C). Since CDDP3 is soluble in water and stable under chloride ion free conditions, encapsulation of CDDP3 into liposomes at high concentrations as depicted in Fig. 2 should be feasible since the low solubility of CDDP in water impairs encapsulation into liposomes. CDDP3 was encapsulated into liposomes with SLX and the conversion to CDDP in the presence of chloride ions was monitored as the chemical shift (δ) by ^{195}Pt NMR. The chemical shifts of ^{195}Pt were referenced to sodium hexachloroplatinate ($\delta = 0$ ppm). After incubation of CDDP3-encapsulated liposomes with chloride ion for 96 h, the chemical shift (δ) indicated only −2160 ppm, which is identical to the chemical shift (δ) of CDDP (Fig. 3). No chemical shift of CDDP3 ($\delta = -1620$ ppm) was detected indicating that CDDP3 in SLX liposomes efficiently converted to CDDP in the presence of chloride ions. The chemical shifts of −1620 ppm and −2160 ppm are consistent with those of CDDP3 and CDDP, respectively, as described by Rosenberg (1978).

3.2. Characterization of CDDP liposomes prepared from CDDP3

Encapsulation of CDDP in liposomes under various conditions was summarized in Table 1. When encapsulation was started with

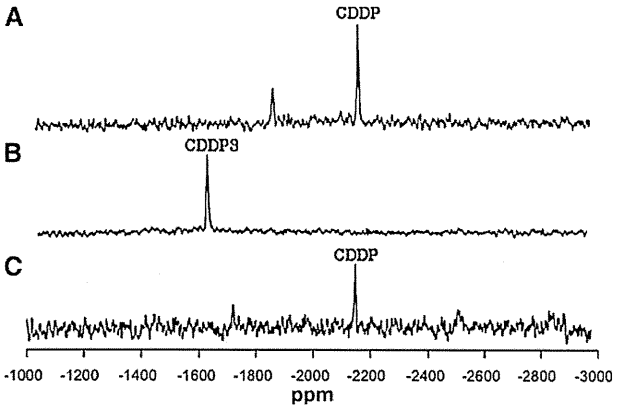

Fig. 3. Conversion of CDDP3 in the liposomes with SLX to CDDP detected by ^{195}Pt NMR. (A) 6.6 mM of CDDP in deuterium oxide; (B) 137 mM of CDDP3 in deuterium oxide; (C) CDDP3 encapsulated liposomes with SLX were treated with 150 mM NaCl for 96 h.

10 mg of CDDP3 and 4.5 mg of lipid, the resultant quantity of CDDP incorporated into SLX-Lip was 211 μg CDDP/3.5 mg lipid/mL and the loading efficiency was 6×10^{-2}. It is important to note that the quantity of CDDP in SLX-Lip increased from 211 μg to 821 μg depending on the amount of lipid. However, it was difficult to make the encapsulation efficiency higher than 10%. Since we found the loading efficiency was almost constant during the course of experiment, we took the loading efficiency as a parameter specific to the encapsulation method. On the other hand, the quantity of CDDP in SLX-Lip was 0.7 μg CDDP/3.5 mg lipid/mL and the loading efficiency was 2×10^{-3} when CDDP was directly encapsulated into liposomes. Actually 1.4 mg was the maximum amount of CDDP for encapsulation while 10 mg was available for CDDP3 in a similar condition. Thus, CDDP3 dramatically improved CDDP encapsulation by almost 300 times in quantity and 42 times in encapsulation efficiency when compared with direct encapsulation of CDDP into liposomes at the initial lipid amount of 4.5 mg. The CDDP loading efficiency appeared to be improved 30 times. The CDDP loading efficiency was improved by almost 4 times when compared with that of 1.4×10^{-2} for SPI-077 (Harrington et al., 2001; Kim et al., 2001). We successfully concentrated CDDP-SLX-Lip and CDDP-Lip up to 4.2 mg CDDP/70 mg lipid/mL, which was 20 times more than the concentration of CDDP in SPI-077. Dynamic laser scattering of the CDDP-SLX-Lip prepared from CDDP3 showed a mean diameter of about 160 nm (Table 1). The ζ potential of the liposomes was negative irrespective of the material of encapsulation (Table 1). Even after 6 months of storage at 4 °C, the leakage of CDDP from liposomes was only about 6% of the total amount of CDDP incorporated into liposomes just after preparation.

3.3. In vivo acute toxicity

The acute toxicity of CDDP-SLX-Lip was evaluated in normal mice by injection via tail veins. The mice were observed for 14 days after injection. The survival rate was 75% when mice received CDDP-SLX-Lip at doses of 18 or 25 mg CDDP/kg body weight. In contrast, the survival rates were 25% and 0% when mice received CDDP at doses of 18 and 25 mg CDDP/kg body weight, respectively (Fig. 4A). The mice did not die when they received empty liposomes with SLX. From these results encapsulation of CDDP in liposomes was found remarkably effective to protect mice from toxicity. This effect of encapsulation was not only recognized in the survival rate but also in the loss of body weight. When CDDP was administered at doses of 18 mg CDDP/kg body weight and 25 mg CDDP/kg body weight, the loss of body weight was 20% during 5 days and 25% during 4 days, respectively. The mice, which received CDDP-SLX-Lip at

Table 1
Physicochemical characteristics of CDDP liposomes prepared with CDDP or CDDP3 ($n = 3$).

	Method of encapsulation			
	I[a]	II[b]		
CDDP (mg)[c]	1.4	0	0	0
CDDP3 (mg)[c]	0	10	10	10
Lipid (mg)[c]	4.5	4.5	9	18
Lipid concentration (mg/mL)[d]	3.5 ± 0.4	3.5 ± 0.3	7.8 ± 0.5	16.5 ± 0.8
Particle size (nm)[e]	158 ± 6.5	150 ± 5.7	152 ± 5.5	160 ± 6.2
ζ potential (mV)	−57 ± 5.3	−55 ± 2.8	−50 ± 3.8	−54 ± 5.2
CDDP concentration (μg/mL)[f]	0.7 ±0.2	211 ± 8	402 ± 0.5	821 ± 0.3
CDDP encapsulation efficiency (%)[g]	0.05	2.11	4.02	8.21
CDDP loading efficiency[h]	2×10^{-3}	6×10^{-2}	5×10^{-2}	5×10^{-2}

[a] Direct encapsulation of CDDP into liposomes.
[b] Encapsulation of CDDP3 into liposomes followed by conversion into CDDP in TAPS buffer containing NaCl.
[c] Initial amount used to prepare 1 mL of CDDP liposome.
[d] Total cholesterol in CDDP liposome solution was measured using a Determiner TC555 Kit.
[e] Measured by photon correlation spectroscopy with a Nano-S90 (Malvern). Polydispersity index was between 0.1 and 0.5 in each case.
[f] The amount of platinum was measured and the amount of CDDP was calculated as defined by Eq. (2) in Section 2.7.
[g] Encapsulation efficiency was calculated as defined by Eq. (3) in Section 2.7.
[h] Loading efficiency was calculated as defined by Eq. (4) in Section 2.7.

the dose of 18, 25 and 50 mg CDDP/kg body weight, showed the loss of body weight by about 15% during 3 days and recovered the loss by less than 10% during 5 days (Fig. 4B). Liposomes without CDDP had no significant effect on the body weight. These results support the possibility that CDDP-SLX-Lip can significantly reduce the toxicity of CDDP *in vivo*.

3.4. Effect of CDDP-SLX-Lip on normal tissues

The effect of CDDP-SLX-Lip and CDDP on normal tissues of mice was histologically evaluated (Fig. 5). Kidney, spleen and liver were excised from mice, which received a dose of 25 mg CDDP/kg body weight. Since mice died at day 4 from the injection of CDDP, tissues were prepared at day 4 after injection. Tissues were stained with HE and by TUNEL method to assess for apoptosis. Abnormal changes were not found in the kidney in mice which received both CDDP-SLX-Lip and CDDP (Fig. 5a,c) but TUNEL positive tubular epithelial cells were sporadically detected after CDDP treatment (Fig. 5d). CDDP-SLX-Lip treatment also did not produce any abnormal changes in the spleen (Fig. 5e,f). However, CDDP treatment of mice induced atrophy of the follicles with necrosis and a decrease in cell number in the white pulp (Fig. 5g). In follicles, phagocytosed dead lymphocytes were observed. TUNEL positive cells were also found in the white pulp (Fig. 5h). In liver, abnormal cells and TUNEL positive cells were not found after the administration of either CDDP-SLX-Lip (Fig. 5i,j) or CDDP (Fig. 5k,l).

3.5. Induction of E-selectin on HUVEC by EAT cells

Since SLX can bind to E-selectin, it is important to ascertain whether E-selectin expression occurs or can be induced on vascular endothelial cells in the tumor to validate tumor targeting. As shown in Fig. 6, E-selectin expression was induced on HUVEC, when stimulated by TNF-α. Although not all tumors may produce TNF-α, it is possible that tumors should express multiple cytokines, which can through a paracrine mechanism induce E-selectin expression on surrounding endothelial cells. The conditioned medium of EAT cells was in fact able to induce E-selectin expression on HUVEC in vitro while control medium did not (Fig. 6).

3.6. Expression of E-selectin on vascular endothelial walls in tumor

The thin section prepared from the solid EAT tissue was subjected to the assessment for the expression of E-selectin on vascular endothelial walls in the tumor. As shown in Fig. 7, E-selectin and blood vessels in the section were stained with anti-E-selectin antibody and LEL, which has specific affinity to fucose on the vascular endothelial cells. Since the sites of E-selectin expression agreed well with vascular walls, the vascular endothelial cells were judged to express E-selectin in the tumor tissue. These results as well as those in HUVEC suggest that the angiogenic vascular endothelial cells in EAT can be stimulated by cytokines or factors that are secreted from EAT cells to induce E-selectin expression.

3.7. Accumulation of CDDP in tumors

We previously reported that the accumulation of liposomes with SLX in the tumor was highest at 48 h after injection when evaluated by *in vivo* imaging using Cy5.5-encapsulated liposomes with SLX (Hirai et al., 2007a). On the basis of these data, the accumulation of CDDP-SLX-Lip in tumors was evaluated at 48 h after injection. CDDP-SLX-Lip or CDDP-Lip were independently administrated into the tail veins of mice bearing EAT tumors. The accumulation of CDDP in the tumors was evaluated by the amount of platinum derived from CDDP at 48 h after injection. The accumulation of CDDP from CDDP-SLX-Lip in the tumors was 6 times higher than that by CDDP-Lip indicating the potential targeting ability of CDDP-SLX-Lip *in vivo* (Fig. 8).

3.8. Antitumor effect of CDDP-SLX-Lip in vivo

The antitumor effect of CDDP-Lip and CDDP-SLX-Lip was evaluated in a mouse xenograft model of A549 lung carcinoma cells because CDDP is widely used for the treatment of lung carcinoma. When CDDP was administrated at 25 mg/kg body weight, all mice died at day 4 after injection. The volume of the tumors that were exposed to either CDDP-Lip or CDDP-SLX-Lip was significantly smaller than that of the non-treated tumors. A difference in tumor volumes between the two different CDDP containing liposomes could not be detected until 12 days after injection. CDDP-SLX-Lip suppressed the growth of tumors much more effectively than CDDP-Lip 19–26 days after injection. Suppression of tumor growth by CDDP-Lip (arrow a in Fig. 9) could be attributed to an enhanced permeability and retention effect (EPR). Further suppression induced by CDDP-SLX-Lip (arrow b in Fig. 9) might be accounted for by the effect of active targeting through the binding of SLX to the tumor vascular endothelial cells.

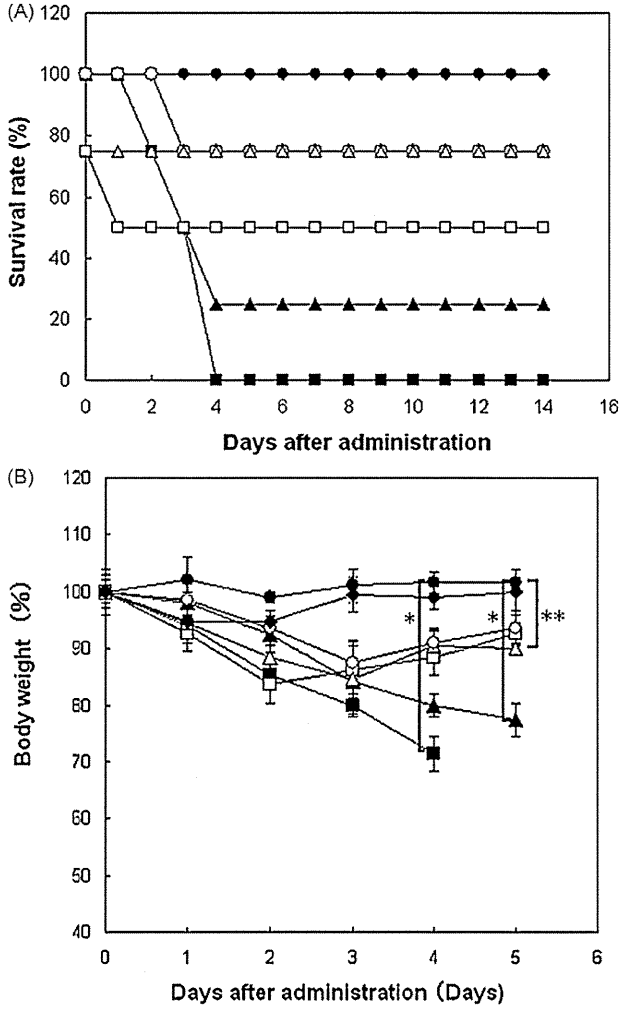

Fig. 4. Survival rate and body weight change of normal mice that received CDDP-SLX-Lip. (A) Survival rate (%); (B) body weight (%). Keys: ▲, CDDP solution (18 mg CDDP/kg body weight); ■, CDDP solution (25 mg CDDP/kg body weight); ○, CDDP-SLX-Lip (18 mg CDDP/kg body weight); △,CDDP-SLX-Lip (25 mg CDDP/kg body weight); □, CDDP-SLX-Lip (50 mg CDDP/kg body weight); ♦, empty liposomes; ●, saline solution. Each sample was injected into normal mice (female, 8 weeks) via tail veins. Results are expressed as the mean ($n=4$); bars, ±SE. *$P<0.005$; **not significant ($P>0.05$).

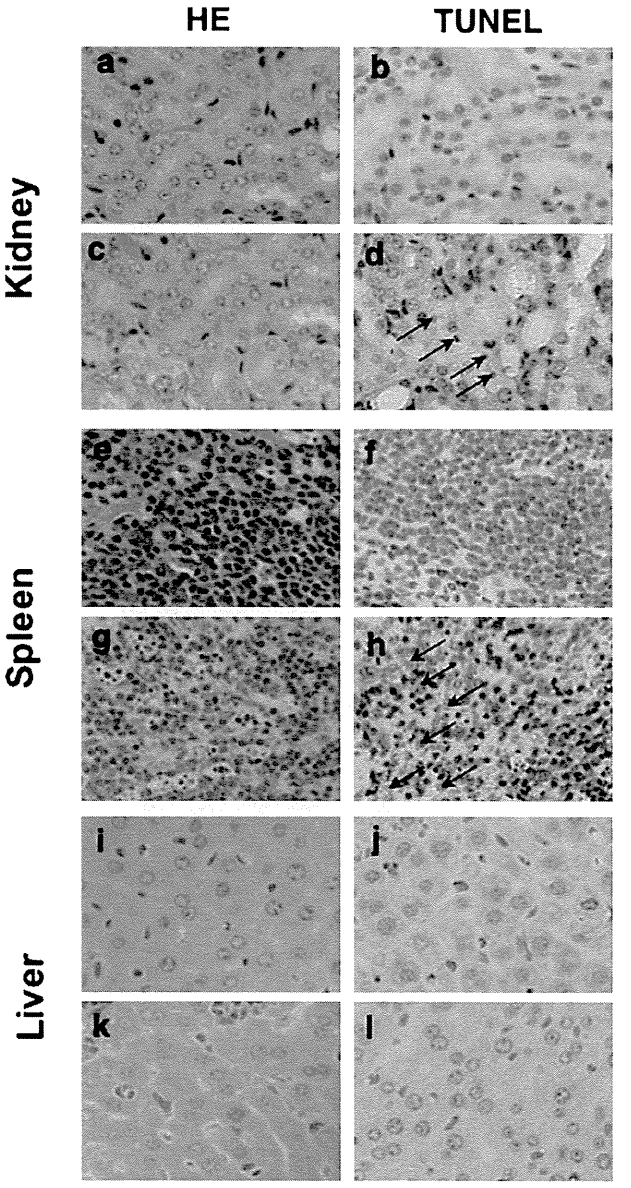

Fig. 5. Histochemical analysis of organs, which received CDDP and CDDP-SLX-Lip. CDDP-SLX-Lip (a, b, e, f, i, j) or CDDP (c, d, g, h, k, l) was injected into each normal mouse (Balb/c, female, 8-week-old) via tail veins at the dose of 25 mg CDDP/kg body weight. At 3 days after administration, kidney (a, b, c, d), spleen (e, f, g, h) and liver (i, j, k, l) were excised and fixed. HE staining (a, c, e, g, i and k) and TUNEL immunohistochemical staining (b, d, f, h, j and l) of the slices were observed. Black arrows indicate TUNEL positive cells. Objective lens was 60×.

4. Discussion

Here we have established a simple and novel method to encapsulate CDDP into liposomes at significantly high concentrations. We then applied this methodology to generate liposomes containing SLX to selectively target tumors and to substantially eliminate or reduce the deleterious and toxic side effects of high dose of CDDP. To achieve high concentrations of CDDP that could be encapsulated into liposomes, we chose to use CDDP3. Since CDDP3 is a hydrophilic derivative of CDDP and readily converts to CDDP in the presence of chloride ions (Fig. 1C), the entire encapsulation procedure could be executed in an aqueous phase. As shown in Fig. 2, CDDP3 was first dissolved at a saturated concentration in a buffer without chloride ions and encapsulated into liposomes. CDDP3 in the liposomes was then converted into CDDP by replacing buffer with buffer containing 150 mM NaCl. As the result, the CDDP encapsulation efficiency and the CDDP loading efficiency were drastically improved when compared with the conventional method of directly encapsulating CDDP. The CDDP loading efficiency in CDDP-SLX-Lip was improved by almost 4 times even when compared with the antecedent CDDP liposome, SPI-077 (Harrington et al., 2001; Kim et al., 2001). The amount of CDDP encapsulated in this study was considerably higher than could be accounted for by the enhanced solubility of CDDP3 in water as compared to CDDP. The negatively charged surface of the liposomes was designed to avoid being bound by blood proteins, such as opsonin, as well as to enhance the retention in blood. CDDP3 in aqueous solution is positively charged, so that it is conceivable that CDDP3 can be electrostatically bound to negatively charged lipids when encapsulated into liposomes.

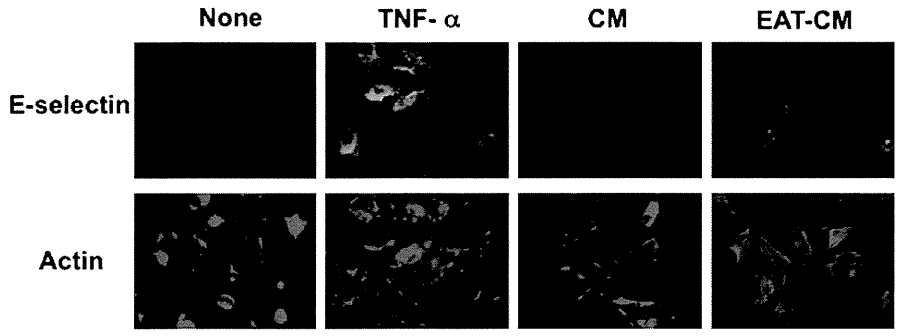

Fig. 6. Evaluation of E-selectin expressed on HUVEC. Cells were cultured in medium for HUVEC supplemented 10% FBS (None), or with 10 ng/mL of TNF-α (TNF-α), in DMEM supplemented 10% FBS (CM), or with EAT cultured DMEM supplemented 10% FBS (EAT-CM) for 4 h. To detect E-selectin, anti-E-selectin antibody was used followed by FITC labeled anti-mouse IgG polyclonal antibody (E-selectin). Actin filaments were stained with rhodamine labeled phalloidin (Actin). The magnification was 40×.

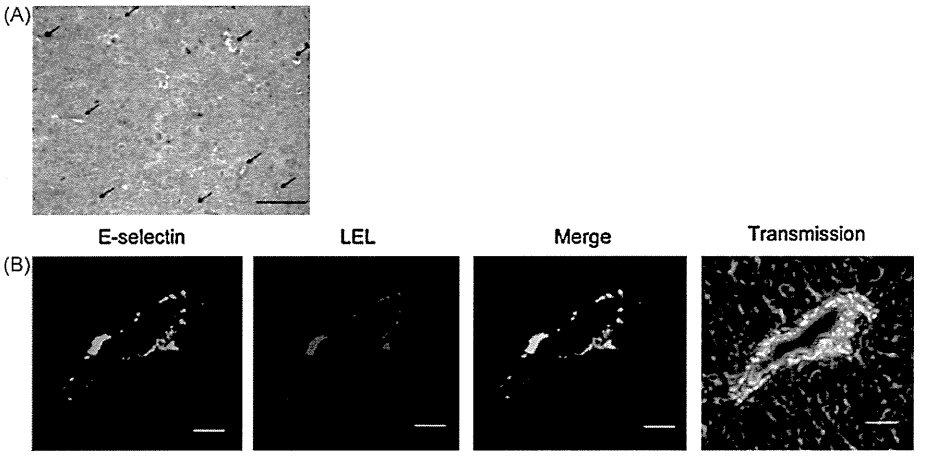

Fig. 7. The expression of E-selectin in vascular vessels of solid EAT. (A) HE staining of the section. Arrows indicated locations of vascular vessels. Scale bar: 100 μm. (B) Vascular vessel stained for E-selectin and for LEL. After deparaffinized, the section was incubated with anti-E-selectin antibody (10 μg/mL) for 1 h at 37 °C, then incubated with FITC labeled goat anti-mouse IgG and LEL conjugated with Texas red for 1 h at room temperature. Merge, colocalization of E-selectin and vascular endothelial cells was shown in yellow. Scale bar showed 20 μm.

The mean diameter of CDDP-SLX-Lip particle in the present study was about 160 nm (Table 1). Due to the SLX moiety, CDDP-SLX-Lip more than likely bind to the E-selectin on tumor vascular endothelial cells where they may enter the gaps between endothelial cells of the capillary bed, which are in the range of 100–300 nm and thereby penetrate into the tumor (Drummond et al., 1999; Gabizon, 1992; Huang et al., 1992, 1993; Wu et al., 1993).

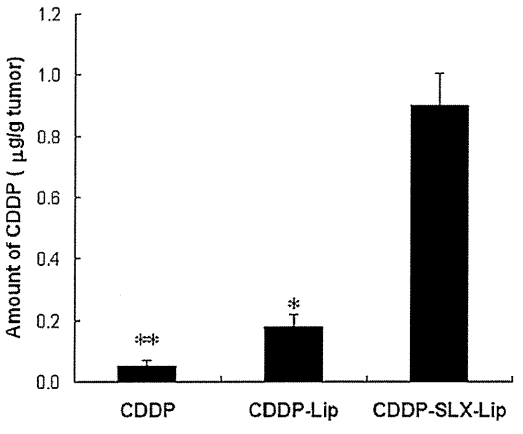

Fig. 8. Accumulation of CDDP in the tumor in vivo. At day 10 after transplantation of EAT cells, CDDP-SLX-Lip, CDDP-Lip or CDDP (2 mg/kg body weight as CDDP) were administered from tail veins of mice. At 48 h after injection the tumor tissues were excised and the amount of platinum were measured by FAAS. Results are expressed as the mean ± SD ($n = 3$). *$P < 0.01$ compared with CDDP-Lip. **$P < 0.005$ compared with CDDP.

CDDP-SLX-Lip were evaluated *in vivo* for acute toxicity and antitumor activity with target potential. The acute toxicity of CDDP was apparently and remarkably reduced by the encapsulation of CDDP in SLX liposomes. When CDDP was injected at 25 mg CDDP/kg body weight, significant toxicity in the kidney was not obvious by HE staining (Fig. 5c) and the TUNEL assay showed only a small number of positive cells in kidney (Fig. 5d). In this part of the study, the period between administration of CDDP and removal of tissues was 3 days, which was probably too short for CDDP to exhibit any significant nephrotoxicity. To observe more dramatic nephrotoxic effects of CDDP, it would probably require longer periods of administration at lower doses of CDDP. As for the acute toxicity, we can conclude that CDDP-SLX-Lip are relatively safe as drug when compared to CDDP with an excellent survival rate as shown in Fig. 4. It is noteworthy that CDDP-SLX-Lip loading of 25 mg CDDP/kg body weight showed significant antitumor activity in vivo (Fig. 9). While an EPR effect should allow the accumulation of CDDP-Lip in tumors (Matsumura and Maeda, 1986) active targeting by CDDP-SLX-Lip exhibited an additive effect. In this context, CDDP-SLX-Lip were more effective than CDDP-Lip at 19 and 26 days after administration (Fig. 9). The accentuated antitumor activity appearing in the late stages may be related to leakage of CDDP from CDDP-SLX-Lip into the tumor. Furthermore, the expression of E-selectin on tumor vascular endothelial cells may be upregulated by tumor-

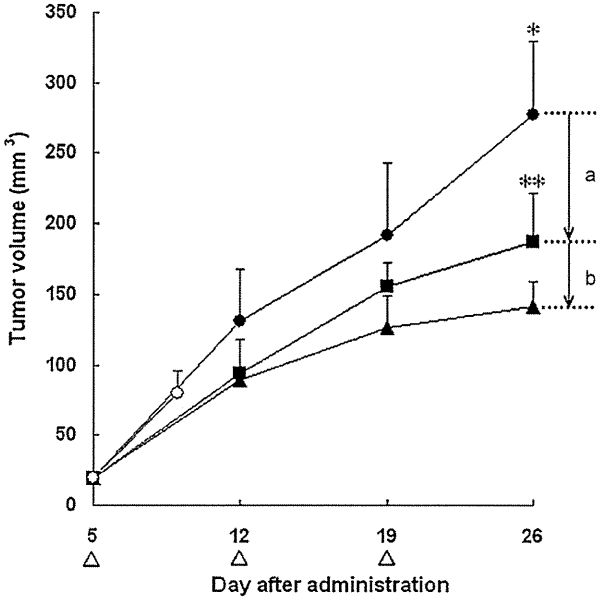

Fig. 9. Comparison of tumor growth suppression with CDDP-SLX-Lip, CDDP-Lip and CDDP in A549-bearing mice. Keys: ▲, CDDP-SLX-Lip (25 mg CDDP/kg body weight); ■,CDDP-Lip (25 mg CDDP/kg body weight); ○, CDDP solution (25 mg CDDP/kg body weight); ●, saline. Each sample was injected via tail veins of A549-bearing mice on days 5, 12 and 19 after tumor cell transplantation. At each day of 5, 12, 19 and 26 after transplantation, each tumor volume (mm^3) was measured. Each open triangle at the horizontal axis shows the time of administration. Results are expressed as the mean ± SD ($n = 4$). *$P < 0.01$ compared with saline. **$P < 0.05$ compared with CDDP-Lip. Vertical arrows indicate the effects of EPR (a) and active targeting (b).

derived vascular endothelial cell growth factor (VEGF) (Aoki et al., 2001), which could account for the enhanced antitumor activity of CDDP-SLX-Lip versus CDDP-Lip. CDDP-SLX-Lip might therefore be more effective than unconjugated CDDP on a wide range of tumors because a number of tumors are sensitive to VEGF-induced angiogenesis (Szekanecz et al., 1999).

Recently, the number of E-selectin-positive vessels was found to be higher in invasive micropapillary breast carcinoma than in invasive ductal carcinoma which was correlated with histological grade (Wei et al., 2008). Furthermore, TNF-α expression, which is known to induce E-selectin in vascular endothelial cells (Murakami et al., 2000), showed a significant positive correlation with the rate of proliferation, histological grade, lymph node metastasis and microvessel density (Cui et al., 2008). Targeting E-selectin should be a feasible and practical therapeutic strategy for breast carcinoma with poor prognosis. Further detailed studies such as distribution, clearance, toxicity, application for various tumor cells and doses with CDDP-SLX-Lip are underway.

5. Conclusion

We successfully established a novel efficient technology to encapsulate CDDP in liposomes at high concentrations. Targeting E-selectin on the vascular endothelial cells in tumor tissues by using CDDP-SLX-Lip should be effective in providing for selective tumor uptake.

The increased loading efficiency of CDDP together with the ability of targeting E-selectin are expected to enhance the pharmaceutical availability of CDDP and to improve the therapeutic index.

CDDP-SLX-Lip should provide a way of developing novel antitumor therapy with CDDP, decreasing the side effects without sparing the antitumor activity.

Acknowledgements

We thank Prof. T. Ema (Okayama University) for his kind support and helpful advises in measuring Pt content of CDDP by NMR and Prof. L. Fu (Tianjin Medical School) for helpful discussions.

References

Aoki, M., Kanamori, M., Yudoh, K., Ohmori, K., Yasuda, T., Kimura, T., 2001. Effects of vascular endothelial growth factor and E-selectin on angiogenesis in the murine metastatic RCT sarcoma. Tumour Biol. 22, 239–246.
Bandak, S., Goren, D., Horowitz, A., Tzemach, D., Gabizon, A., 1999. Pharmacological studies of cisplatin encapsulated in long-circulating liposomes in mouse tumor models. Anticancer Drugs 10, 911–920.
Bevilacqua, M.P., Stengelin, S., Gimbrone Jr., M.A., Seed, B., 1989. Endothelial leukocyte adhesion molecule 1: an inducible receptor for neutrophils related to complement regulatory proteins and lectins. Science 243, 1160–1165.
Borch, R.F., Markman, M., 1989. Biochemical modulation of cisplatin toxicity. Pharmacol. Ther. 41, 371–380.
Comis, R.L., 1994. Cisplatin: the future. Semin. Oncol. 21, 109–113.
Cui, L.F., Guo, X.J., Wei, J., Liu, F.F., Fan, Y., Lang, R.G., Gu, F., Zhang, X.M., Fu, L., 2008. Overexpression of TNF-α and TNFRII in invasive micropapillary carcinoma of the breast: clinicopathological correlations. Histopathology 53, 381–388.
Cvitkovic, E., Spaulding, J., Bethune, V., Martin, J., Whitmore, W.F., 1977. Improvement of *cis*-dichlorodiammineplatinum therapeutic index in an animal model. Cancer 39, 1357–1361.
Dhara, S., 1970. A rapid method for the synthesis of *cis*-[$Pt(NH_3)Cl_2$]. Indian J. Chem. 7, 193–194.
Drummond, D.C., Meyer, O., Hong, K., Kirpotin, D.B., Papahadjopoulos, D., 1999. Optimizing liposomes of chemotherapeutic agents to solid tumors. Pharmacol. Rev. 51, 691–743.
Gabizon, A.A., 1992. Selective tumor localization and improved therapeutic index of anthracyclines encapsulated in long-circulating liposomes. Cancer Res. 52, 891–896.
Goldstein, R.S., Noordewier, B., Bond, J.T., Hook, J.B., Mayor, G.H., 1981. *cis*-Dichlorodiammineplatinum nephrotoxicity: time course and dose response of renal functional impairment. Toxicol. Appl. Pharmacol. 60, 163–175.
Harrington, K.J., Lewanski, C.R., Northcote, A.D., Whittaker, J., Wellbank, H., Vile, R.G., Peters, A.M., Stewart, J.S., 2001. Phase I–II study of pegylated liposomal cisplatin (SPI-077) in patients with inoperable head and neck cancer. Ann. Oncol. 12, 493–496.
Hayes, D.M., Cvitkovic, E., Golbey, R.B., Scheiner, E., Helson, L., Krakoff, I.H., 1977. High dose *cis*-platinum diammine dichloride: amelioration of renal toxicity by mannitol diuresis. Cancer 39, 1372–1381.
Hirai, M., Minematsu, H., Kondo, N., Oie, K., Igarashi, K., Yamazaki, N., 2007a. Accumulation of liposome with Sialyl Lewis X to inflammation and tumor region: application to in vivo bio-imaging. Biochem. Biophys. Res. Commun. 353, 553–558.
Hirai, M., Oie, K., Igarashi, K., 2007b. In vivo imaging reagent with liposome with sugar chain. Med. Sci. Digest. 33, 826–828.
Huang, S.K., Mayhew, E., Gilani, S., Lasic, D.D., Martin, F.J., Papahadjopoulos, D., 1992. Pharmacokinetics and therapeutics of sterically stabilized liposomes in mice bearing C-26 colon carcinoma. Cancer Res. 52, 6774–6781.
Huang, S.K., Martin, F.J., Jay, G., Vogel, J., Papahadjopoulos, D., Friend, D.S., 1993. Extravasation and transcytosis of liposomes in Kaposi's sarcoma-like dermal lesions of transgenic mice bearing the HIV tat gene. Am. J. Pathol. 143, 10–14.
Kim, E.S., Lu, C., Khuri, F.R., Tonda, M., Glisson, B.S., Liu, D., Jung, M., Hong, W.K., Herbst, R.S., 2001. A phase II study of STEALTH cisplatin (SPI-077) in patients with advanced non-small cell lung cancer. Lung Cancer 34, 427–432.
Lee, C.M., Tanaka, T., Murai, T., Kondo, M., Kimura, J., Su, W., Kitagawa, T., Ito, T., Matsuda, H., Miyasaka, M., 2002. Novel chondroitin sulfate-binding cationic liposomes loaded with cisplatin efficiently suppress the local growth and liver metastasis of tumor cells in vivo. Cancer Res. 62, 4282–4288.
Legha, S.S., Hodges, C., Ring, S., 1992. Efficacy of ondansetron against nausea and vomiting caused by dacarbazine containing chemotherapy. Cancer 70, 2018–2020.
Liu, F.T., Rabinovich, G.A., 2005. Galectins as modulators of tumor progression. Nat. Rev. Cancer 5, 29–41.
Matsumura, Y., Maeda, H., 1986. A new concept for macromolecular therapeutics in cancer chemotherapy: mechanism of tumoritropic accumulation of proteins and the antitumor agent smancs. Cancer Res. 46, 6387–6392.
Mayer, B., Spatz, H., Funke, I., Johnson, J.P., Schildberg, F.W., 1998. De novo expression of the cell adhesion molecule E-selectin on gastric cancer endothelium. Langenbeck's Arch. Surg. 383, 81–86.
Meerum Terwogt, J.M., Groenewegen, G., Pluim, D., Maliepaard, M., Tibben, M.M., Huisman, A., ten Bokkel Huinink, W.W., Schot, M., Welbank, H., Voest, E.E., Beijnen, J.H., Schellens, J.M., 2002. Phase I and pharmacokinetic study of SPI-77, a liposomal encapsulated dosage form of cisplatin. Cancer Chemother. Pharmacol. 49, 201–210.
Murakami, T., Mataki, C., Nagao, C., Umetani, M., Wada, Y., Ishii, M., Tsutsumi, S., Kohro, T., Saiura, A., Aburatani, H., Hamakubo, T., Kodama, T., 2000. The gene expression profile of human umbilical vein endothelial cells stimulated by tumor necrosis factor alpha using DNA microarray analysis. J. Atheroscler. Thromb. 7, 39–44.

Navari, R.M., Kaplan, H.G., Gralla, R.J., Grunberg, S.M., Palmer, R., Fitts, D., 1994. Efficacy and safety of granisetron, a selective 5-hydroxytryptamine-3 receptor antagonist, in the prevention of nausea and vomiting induced by high-dose cisplatin. Clin. Oncol. 12, 2204–2210.

Newman, M.S., Colbern, G.T., Working, P.K., Engbers, C., Amantea, M.A., 1999. Comparative pharmacokinetics, tissue distribution, and therapeutic effectiveness of cisplatin encapsulated in long-circulating, pegylated liposomes (SPI-077) in tumor-bearing mice. Cancer Chemother. Pharmacol. 43, 1–7.

Ogilvie, G.K., Fettman, M.J., Jameson, V.J., Walters, L.M., Lafferty, M.H., Cooper, M.F., Powers, B.E., Ciekot, P.A., Atwater, S.W., Withrow, S.J., 1992. Evaluation of a one-hour saline diuresis protocol for administration of cisplatin to dogs. Am. J. Vet. Res. 53, 1666–1669.

Rosenberg, B., 1978. Platinum complex–DNA interactions and anticancer activity. Biochimie 60, 859–867.

Szekanecz, Z., Halloran, M.M., Haskell, C.J., Shah, M.R., Polverini, P.J., Koch, A.E., 1999. Mediators of angiogenesis: the role of cellular adhesion molecules. Trends Glycosci. Glycotechnol. 11, 73–93.

Vaage, J., Donovan, D., Wipff, E., Abra, R., Colbern, G., Uster, P., Working, P., 1999. Therapy of a xenografted human colonic carcinoma using cisplatin or doxorubicin encapsulated in long-circulating pegylated stealth liposomes. Int. J. Cancer 80, 134–137.

Veal, G.J., Griffin, M.J., Price, E., Parry, A., Dick, G.S., Little, M.A., Yule, S.M., Morland, B., Estlin, E.J., Hale, J.P., Pearson, A.D., Welbank, H., Boddy, A.V., 2001. A phase I study in paediatric patients to evaluate the safety and pharmacokinetics of SPI-77, a liposome encapsulated formulation of cisplatin. Br. J. Cancer 84, 1029–1035.

Vestweber, D., Blanks, J.E., 1999. Mechanisms that regulate the function of the selectins and their ligands. Physiol. Rev. 79, 181–213.

Von Hoff, D.D., Schilsky, R., Reichert, C.M., Reddick, R.L., Rozencweig, M., Young, R.C., Muggia, F.M., 1979. Toxic effects of *cis*-dichlorodiammineplatinum (II) in man. Cancer Treat. Rep. 63, 1527–1531.

Wei, J., Cui, L., Liu, F., Fan, Y., Lang, R., Gu, F., Guo, X., Tang, P., Fu, L., 2008. E-selectin and Sialyl Lewis X expression is associated with lymph node metastasis of invasive micropapillary carcinoma of the breast. Int. J. Surg. Pathol. [Epub ahead of print].

Wu, N.Z., Da, D., Rudoll, T.L., Needham, D., Whorton, A.R., Dewhirst, M.W., 1993. Increased microvascular permeability contributes to preferential accumulation of Stealth liposomes in tumor tissue. Cancer Res. 53, 3765–3770.

Yamazaki, N., 1989. Analysis of the carbohydrate-binding specificity of lectin-conjugated lipid vesicles, which interact with polysaccharide, fragments. J. Membr. Sci. 41, 249–267.

Yamazaki, N., Kodama, M., Gabius, H.-J., 1994. Neoglycoprotein–liposome and lectin–liposome conjugates as tools for carbohydrate recognition research. Methods Enzymol. 242, 56–65.

Biotechnol Lett (2010) 32:361–366
DOI 10.1007/s10529-009-0160-9

ORIGINAL RESEARCH PAPER

Production of biologically active IgG hinge-tag soluble epidermal growth factor receptors (ErbB)

Takayuki Otani · Toshihiro Hashizume · Tadahiro Nagaoka · Tomoko Fukuda · Careen K. Tang · David S. Salomon · Masaharu Seno

Received: 15 September 2009 / Revised: 18 October 2009 / Accepted: 22 October 2009 / Published online: 7 November 2009

Abstract The extracellular domains (ECD) of epidermal growth factor receptors, ErbB1, 2, 3 and 4, were designed as soluble dimeric forms. Each ECD was fused to a short hinge region derived from IgG, such that the stable dimer could be formed with disulfide bridges. This hinge-tagged design minimized the molecular weight to approximately 50% of the conventional Fc-fusion design without an Fc domain of IgG. The refolded dimers could be easily analyzed and characterized by SDS-PAGE. Hinge-tagged soluble ErbBs demonstrated significant affinity for betacellulin and heregulin. The IgG hinge-tag should be a simple method to design soluble dimers that would be useful for high throughput screening of ligands, antagonists or derivatives.

Keywords Epidermal growth factor receptors · ErbB · Extracellular domain · Hinge region · Homodimer · Soluble receptor

Takayuki Otani, Toshihiro Hashizume and Tadahiro Nagaoka equally contributed to this paper.

T. Otani · T. Hashizume · T. Fukuda · M. Seno (✉)
Department of Medical and Bioengineering Science, Graduate School of Natural Science and Technology, Okayama University, 3.1.1 Tsushima-Naka, Kita-ku, Okayama 700-8530, Japan
e-mail: mseno@cc.okayama-u.ac.jp

T. Nagaoka · D. S. Salomon
Tumor Growth Factor Section, Mammary Biology & Tumorigenesis Laboratory, Center for Cancer Research, National Cancer Institute, National Institutes of Health, Bethesda, MD 20892, USA

C. K. Tang
Lombardi Comprehensive Cancer Center, Georgetown University, Washington, DC 20057, USA

Introduction

The epidermal growth factor (EGF) receptor family consists of four members, the EGF receptor (ErbB1), ErbB2, ErbB3, and ErbB4 (Holbro et al. 2003). These receptors play important roles in cellular differentiation, proliferation, transformation and tumorigenesis (Hynes et al. 2001). Each ErbB receptor is a type I transmembrane tyrosine kinase consisting of an extracellular domain (ECD), a transmembrane region and a cytoplasmic domain, which possess tyrosine kinase activity and which is responsible for intracellular signal transduction (Schlessinger 2000). Each ErbB ECD exhibits high affinity to peptides of the EGF-related growth factors that include EGF, TGFα, heregulins (HRG), amphiregulin, betacellulin (BTC), heparin-binding EGF like growth factor (HB-EGF), epiregulin and epigen (Linggi and Carpenter 2006). Upon ligand binding, ErbB receptors undergo homo- and/or hetero-dimerization to induce the intrinsic receptor tyrosine kinase activity, which ultimately results in the simulation of series of intracellular signaling cascades. Soluble ErbB receptors (sErbBs),

which are useful for screening the specificity and the cell surface affinity for ligands and which can inhibit ligands from binding to cognate receptors, have previously been synthesized as proteins between the fusion of the ECD and the Fc domain of IgG (Chamow and Ashkenazi 1996; Fitzpatrick et al. 1998; Jones et al. 1999). Fusion of the Fc domain to the ECD facilitates stable dimer formation which can be purified by affinity chromatography with a protein A coupled gel matrix. However, it is extremely difficult to distinguish dimers from higher order oligomers by conventional SDS-PAGE due to the high molecular weight of the oligomers of the ECD fused to the Fc domain. In this study, we have employed the short hinge region of the Fc domain, which is responsible for the intermolecular disulfide bridges of IgG molecule. This fragment was fused to each of the ECDs of the four ErbBs. The ECD of ErbB1 bound to EGF has the potential for self-dimerization without the transmembrane and cytoplasmic domains (Odaka et al. 1997). Similarly, the ECD of ErbB1 and the ECD of ErbB4 are able to form ligand-activated homodimers in solution (Ferguson et al. 2000). These two reports lead us to assess whether the whole Fc domain of IgG is actually necessary to facilitate dimerization of the ECDs of ErbBs.

Materials and methods

Construction of expression plasmids

cDNAs for the ECD of the ErbB2 and ErbB3 were cloned by RT-PCR from the total RNA of human breast tumor (Clontech) into pCR2.1vector (Invitrogen) respectively. The fragments coding for each ECD were subcloned into pEGFP-N1 (Stratagene) with a FLAG tag epitope. To design sErbB2 and sErbB3 in a dimeric form exploiting disulfide bounds between each hinge region, a synthetic oligo-nucleotide coding for the hinge region of the mouse IgG1 heavy chain (GenBank J00453) 5′-CCGGTGCCCAGGGATTCT GGTTGTAAGCCTTGCATATGTGTA-3′ was inserted into sErbB2-FLAG and sErbB3-FLAG and the expression plasmids for sErbB2-hinge-FLAG and sErbB3-hinge-FLAG were constructed. Human HRGβ2 cDNA was previously described by Tang et al. (1996). To create the expression plasmid for His-HRGβ2-HA, the portion encoding amino acid residues 176–241 corresponding to the EGF motif was inserted into pET14b (Novagen) together with a synthetic oligonucleotide coding for the HA-tag derived from the human influenza hemagglutinin protein. sErbB1 and sErbB4 fused to mouse IgG_1 heavy chain hinge region and His-BTC-HA were described by Nagaoka et al. (2008) in a similar design.

Expression and purification of sErbBs

Either Cos7 cells or HEK293H cells (Gibco) were transformed with each sErbB-hinge-Flag expression plasmid. Transient transformants of Cos7 cells were cultured for 2 days under low serum condition. Transformants of HEK293H cells stably expressing sErbBs were cultured in DMEM containing 30 mM HEPES, pH 7.5, 5% Daigo's GF21 (Nihon Pharmaceutical), 0.5 mg G418/ml and 0.05% Pluronic F-68 (Sigma-Aldrich) at 37°C for 5 days. The cells were then maintained in culture for an additional 5 days in fresh medium. Each sErbB in the medium was purified with an anti-FLAG agarose (Sigma-Aldrich) affinity column. The adsorbed protein was eluted with 0.1 M sodium phosphate buffer, pH 3.5, and the eluted fraction was neutralized with 2 M sodium phosphate buffer, pH 8.0. The buffer was then replaced with PBS by a PD-10 desalting column (GE Healthcare).

Expression and purification of His-HRGβ2-HA and His-BTC-HA

E. coli MM294 (DE3) pLysS (Watanabe et al. 1990) was transformed with the expression vector of His-HRGβ2-HA or His-BTC-HA and each recombinant protein was produced as inclusion bodies. The isolation of inclusion bodies and refolding of the protein was performed as described by Nagaoka et al. (2008). The refolded proteins were purified with a Ni-NTA Superflow column (Qiagen) following the procedure recommended by the manufacturer. The final purity of recombinant protein was evaluated by SDS-PAGE stained with Coomassie Brilliant Blue.

Enzyme immunoassay

The enzyme immunoassay (EIA) was designed to evaluate the affinity of ligands to sErbBs. Each well of a 96-well plate was coated with 100 ng BTC or HRGβ2. Then sErbBs sequentially diluted with PBSB

was added to each well followed by the incubation for 2 h at room temperature. The bound sErbBs were detected with anti-FLAG bioM2 monoclonal antibody coupled with Avidin-HRP conjugate (Zymed Laboratories). The HRP reaction was developed with *o*-phenylenediamine and H_2O_2. After the quench of reaction, absorbance at 492 nm of each well was measured. Each experiment was performed in triplicate.

Competition EIA to estimate Kd value

To estimate dissociation constants (Kd) between HRGβ2 and sErbB3 or sErbB4, competition EIA was performed based on the method described by (Djavadi-Ohaniance et al. 1996). Each well of a 96-well plate was coated with 50 ng HRGβ2. sErbBs were then premixed with varying concentrations of HRGβ2 and added to the wells. The bound sErbBs were detected with HRP labeled anti-FLAG-HRP monoclonal antibody. The HRP reaction was developed with OPD and hydrogen peroxide. After the quench of reaction, absorbance at 492 nm of each well was measured. Each experiment was performed in triplicate.

Western blotting

Proteins were resolved by 5% (v/v) SDS-PAGE and transferred to a PVDF membrane (Bio-Rad). Blots were then probed with anti-FLAG bioM2 monoclonal antibody, anti-HA-tag monoclonal antibody (Roche) or anti-His-tag monoclonal antibody (Cell Signaling) coupled with HRP conjugated Avidin, protein A-HRP (ICN Biomedicals) or anti-mouse IgG polyclonal antibody (Bio-Rad). The HRP signal was developed with Western Lighting and Western Lighting Plus Chemiluminescence Reagent (Perkin Elmer) and exposed to X-ray film (Fuji Film).

Results and discussion

The design of sErbB receptors tagged with the hinge region of mouse IgG tethered to a FLAG-tag epitope is summarized in Fig. 1. When sErbB receptors are designed as a conventional Fc fusion proteins, the molecular weight of the fusion proteins are approximately 120 kDa and the dimers are 240 kDa as listed in Table 1. It is difficult to distinguish these high molecular weight species in conventional procedures such as SDS-PAGE or gel filtration chromatography. In addition, if oligomeric forms are present, it would be even more difficult to distinguish these forms from dimers. On the other hand, the size of the sErbB-hinge-FLAG construct is approx. 70 kDa, which can generate a 140 kDa dimer. These sizes permit for sufficient resolution on SDS-PAGE analysis under non-reducing conditions (Fig. 2a). The size of the hinge-tag region that is fused to each soluble receptor is 1.7 kDa, so that it should not affect the overall size of the ECD (Table 1). Likewise, this construct does not significantly affect the size such that the dimeric forms of each ErbB receptor can be easily resolved and characterized by SDS-PAGE analysis. When the sErbBs that were fused to FLAG-tag with/without the hinge-tag region produced in the culture medium were immunoprecipitated with anti-FLAG antibody, sErbB1, 3 and 4 were found to successfully form dimers only when they were fused to the IgG hinge-tag

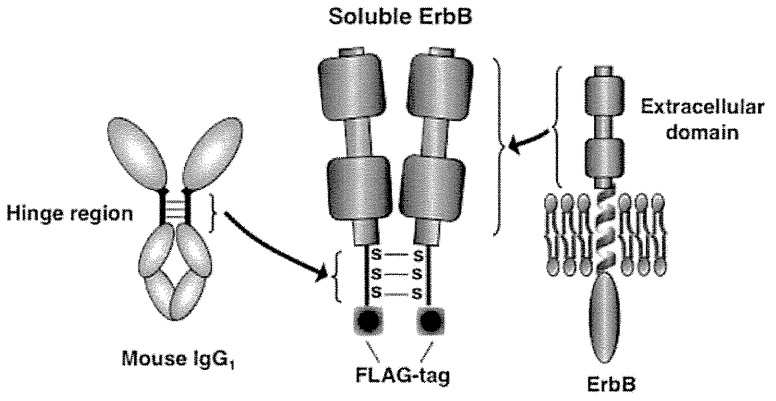

Fig. 1 Schematic drawing of soluble ErbBs with hinge-tag. Hinge region of a mouse IgG_1 was fused to the *C*-terminus of extracellular domain of ErbBs so that they should dimerize into a soluble form via disulfide bridges. Hinge-tag is followed by FLAG-tag at the *C*-terminus for easy detection of the molecule

Table 1 Comparison of molecular weights of sErbB-HF and sErbB-Fc

	Whole (kDa)	ECD (kDa)	sErbB-Fc[a] (kDa)	sErbB-HF[b] (kDa)
ErbB1				
Monomer	132	68.6	118.6	70.3
Homodimer	264	137.2	237.2	140.6
ErbB2				
Monomer	136	69.4	119.4	71.1
Homodimer	272	138.8	238.8	142.2
ErbB3				
Monomer	146	68.7	118.7	70.4
Homodimer	292	137.4	237.4	140.8
ErbB4				
Monomer	145	69.8	119.8	71.5
Homodimer	290	139.6	239.6	143.0

[a] sErbB fused to IgG Fc domain

[b] sErbB fused to hinge-tag and FLAG-tag

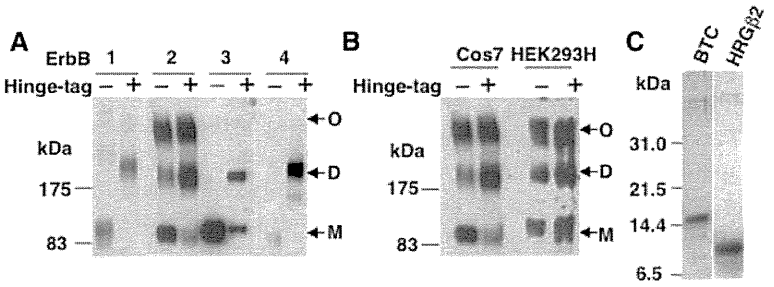

Fig. 2 **a** sErbBs with/without hinge-tags expressed in Cos7 cells. **b** Comparison of sErbB2 produced in Cos7 cells and HEK293H cells. sErbBs in the conditioned media were immunoprecipitated by anti-FLAG agarose and subjected to 5% SDS-PAGE under non-reduced conditions and transferred to PVDF membrane. The blots were probed with anti-FLAG Bio M2 antibody. The positions of monomers (M), dimers (D) and oligomers (O) are shown with *arrows*. **c** Recombinant BTC or HRGβ2 proteins purified to a homogeneity. BTC (MW = 9 kDa) and HRGβ2 (MW = 10 kDa) were produced in *E. coli* with His-tag and HA-tag, purified by Ni-column and subjected to SDS-PAGE under reduced condition. Coomassie Brilliant Blue staining

(Fig. 2a). Although sErbB2 showed oligomeric forms without the hinge-tag region, dimerization of sErbB2 was significantly enhanced with the hinge-tag (Fig. 2a). The oligomeric forms of sErbB2 were observed independently of the cell type, in which they were expressed (Fig. 2b). These oligomeric forms of ErbB2 can easily be reduced to dimeric forms during the purification procedure (data not shown) suggesting that the conformation of the extracellular domain of ErbB2 on the cell surface is labile. This flexible conformation might be a part of conditions that control signal transduction of ErbB2, of which dimerization is independent of ligand binding, resulting in a poor prognosis of cancers when ErbB2 is overexpressed.

For the evaluation of the affinity of the sErbBs to different ligands, recombinant BTC and HRGβ2 were expressed in bacteria and purified to near homogeneity as shown in Fig. 2c. BTC bound to both sErbB1 and sErbB4 in a similar manner (Fig. 3a). HRGβ2 bound to both sErbB3 and sErbB4 showing higher saturation binding to sErbB4 than sErbB3 (Fig. 3b). These ligands did not bind to sErbBs without the hinge-tag region (data not shown). From competition EIA, Kd values for HRGβ2 binding to sErbB3 and sErbB4 were estimated 111 and 51 nM, respectively. These Kd values are close to those previously reported (Fitzpatrick et al. 1998; Jones et al. 1999; Ferguson et al. 2000; Bouyain et al. 2005). Table 2 summarizes Kd values of the ligands and sErbBs together with those described previously. These results suggest that sErbB dimers with hinge-tag have significant binding affinity for BTC and HRGβ2 while the artificial and structurally unrelated peptide ligand EC-1 showed low affinity for sErbB2 (Hashizume et al. 2008). Therefore the full

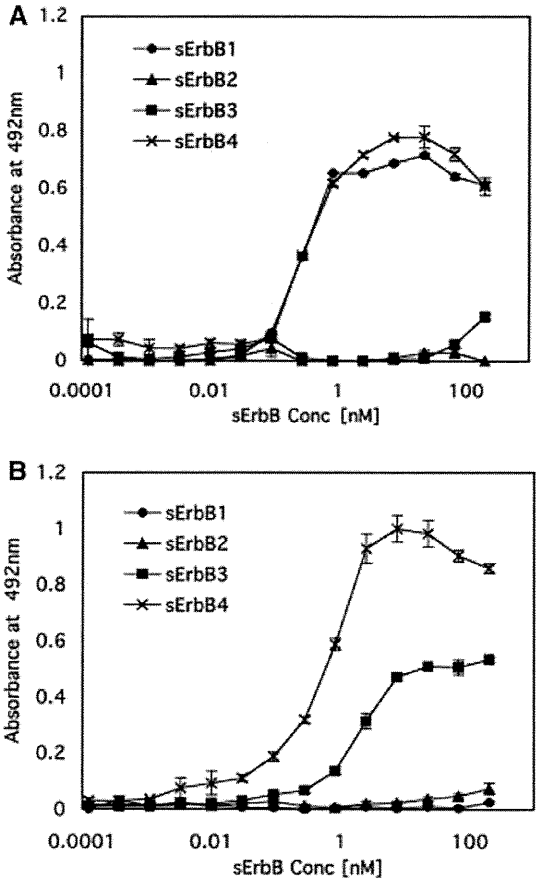

Fig. 3 Binding saturation of BTC (**a**) and HRGβ2 (**b**) assessed by enzyme immunoassay with hinge-tagged sErbBs. Ligands were coated at 100 ng/well in 96 well plate and varying concentration of sErbBs was added. Bound sErbBs were detected with biotinylated anti-FLAG antibody and HRP-avidin. SD was calculated from three independent experiments. Kd values of them were summarized in Table 2

Table 2 Kd values of BTC or HRGβ2 and receptors interaction

Ligand	Kd (nM)			
	sErbB1	sErbB2	sErbB3	sErbB4
BTC	0.35	N.D.[a]	N.D.	3.2
HRGβ2	N.D.	N.D.	111	51
EC-1[b]	N.D.	1.0×10^3	N.D.	N.D.

[a] No significant binding between ligand and sErbB was detected. These results are consistent with the facts that BTC specifically binds to ErbB1 and ErbB4, that HRGβ2 specifically binds to ErbB3 and ErbB4, and that neither of the two binds to ErbB2

[b] Hashizume et al. (2008)

length of Fc domain of IgG is not necessary for the dimerization of the sErbBs and the hinge-tag region should be effective to facilitate sErbB dimerization. These sErbB receptors should be useful for high throughput screening of ligands, antagonists or derivatives.

Acknowledgements We thank Ms. N. Hironaka for the construction of sErbB2 and sErbB3 expression plasmid. This research was partly supported by the Ministry of Education, Culture, Sports, Science and Technology Grant-in-Aid for Scientific Research (B) Nos. 18300164 and 21300179.

References

Bouyain S, Longo PA, Li S, Ferguson KM et al (2005) The extracellular region of ErbB4 adopts a tethered conformation in the absence of ligand. Proc Natl Acad Sci USA 102:15024–15029

Chamow SM, Ashkenazi A (1996) Immunoadhesins: principles and applications. Trends Biotechnol 14:52–60

Djavadi-Ohaniance L, Goldberg ME, Friguet B (1996) Measuring antibody affinity in solution. In: McCafferty J, Hoogenboom HR, Chiswell DJ (eds) Antibody engineering: a practical approach. IRL Press, Oxford, pp 77–98

Ferguson KM, Darling PJ, Mohan MJ et al (2000) Extracellular domains drive homo- but not hetero-dimerization of ErbB receptors. EMBO J 19:4632–4643

Fitzpatrick VD, Pisacane PI, Vandlen RL et al (1998) Formation of a high affinity heregulin binding site using the soluble extracellular domains of ErbB2 with ErbB3 or ErbB4. FEBS Lett 431:102–106

Hashizume T, Fukuda T, Nagaoka T et al (2008) Cell type dependent endocytic internalization of ErbB2 with an artificial peptide ligand that binds to ErbB2. Cell Biol Int 32:814–826

Holbro T, Civenni G, Hynes NE (2003) The ErbB receptors and their role in cancer progression. Exp Cell Res 284:99–110

Hynes NE, Horsch K, Olayioye MA et al (2001) The ErbB receptor tyrosine family as signal integrators. Endocr Relat Cancer 8:151–159

Jones JT, Akita RW, Sliwkowski MX (1999) Binding specificities and affinities of EGF domains for ErbB receptors. FEBS Lett 447:227–231

Linggi B, Carpenter G (2006) ErbB receptors: new insights on mechanisms and biology. Trends Cell Biol 16:649–656

Nagaoka T, Fukuda T, Hashizume T et al (2008) A betacellulin mutant promotes differentiation of pancreatic acinar AR42J cells into insulin-producing cells with low affinity of binding to ErbB1. J Mol Biol 380:83–94

Odaka M, Kohda D, Lax I et al (1997) Ligand-binding enhances the affinity of dimerization of the extracellular domain of the epidermal growth factor receptor. J Biochem 122:116–121

Schlessinger J (2000) Cell signaling by receptor tyrosine kinases. Cell 103:211–225

Tang CK, Perez C, Grunt T et al (1996) Involvement of heregulin-β2 in the acquisition of the hormone-independent phenotype of breast cancer cells. Cancer Res 56:3350–3358

Watanabe T, Seno M, Sasada R et al (1990) Molecular characterization of recombinant human acidic fibroblast growth factor produced in *E. coli*: comparative studies with human basic fibroblast growth factor. Mol Endocrinol 4:869–879

Enhanced Target-Specific Accumulation of Radiolabeled Antibodies by Conjugating Arginine-Rich Peptides as Anchoring Molecules

Rei Miyamoto,[†] Hiromichi Akizawa,[‡] Takeshi Nishikawa,[†] Tomoya Uehara,[†] Yusuke Azuma,[§] Ikuhiko Nakase,[§] Shiroh Futaki,[§] Hirofumi Hanaoka,[∥] Yasuhiko Iida,[⊥] Keigo Endo,[∥] and Yasushi Arano*[,†]

Graduate School of Pharmaceutical Sciences, Chiba University, 1-8-1 Inohana, Chuo-ku, Chiba 260-8675, Japan, Graduate School of Pharmaceutical Sciences, Health Sciences University of Hokkaido, 1757 Kanazawa, Tobetsu-cho, Ishikari-gun, Hokkaido 061-0293, Japan, Institute for Chemical Research, Kyoto University, Gokasho, Uji, Kyoto 611-0011, Japan, Graduate School of Medicine, Gunma University, 39-22, Showa-machi 3-chome, Maebashi, Gunma 371-8511, Japan, and Suzuka University of Medical Science, 1001-1 Kishioka-cho, Suzuka, Mie 510-0293, Japan. Received June 8, 2010; Revised Manuscript Received August 23, 2010

We have devised and estimated a new strategy to prolong the residence time of radiolabeled antibodies in tumor in which an octaarginine peptide (R_8) was used as an anchoring molecule to fix antibodies against CD20 (NuB2; IgG2a) on tumor cells. Conjugation of R_8 with antibodies was performed by maleimide−thiol chemistry using thiol groups generated by reducing the disulfide bonds of the antibody. The R_8-conjugated NuB2 was then reacted with succinimidyl *meta*-[^{125}I]iodobenzoate to prepare [^{125}I]SIB-NuB2$_I$ (0.92 R_8/NuB2) and [^{125}I]SIB-NuB2$_{III}$ (3.38 R_8/NuB2). Both SIB-NuB2$_I$ and SIB-NuB2$_{III}$ exhibited size-exclusion HPLC elution profiles and immunoreactivity to CD20-positive cells similar to those of NuB2. NuB2$_I$ also possessed isoelectric focusing (IEF) profile similar to NuB2. However, NuB2$_{III}$ registered a broad IEF band toward higher pI. When incubated with CD20-positive cells, [^{125}I]SIB-NuB2$_I$ and [^{125}I]SIB-NuB2$_{III}$ exhibited 1.4 and 4.0 times higher cell-associated radioactivity than [^{125}I]SIB-NuB2. After the cells were washed and reincubated in a fresh medium for 3 h, [^{125}I]SIB-NuB2$_I$ and [^{125}I]SIB-NuB2$_{III}$ exhibited significantly higher cell-associated radioactivity than [^{125}I]SIB-NuB2. In biodistribution studies in normal mice, while both [^{125}I]SIB-NuB2$_I$ and [^{125}I]SIB-NuB2 exhibited similar biodistribution profiles, [^{125}I]SIB-NuB2$_{III}$ showed faster clearance from the blood and higher hepatic radioactivity levels than [^{125}I]SIB-NuB2. In SCID mice bearing CD20-positive xenografts, [^{131}I]SIB-NuB2$_I$ exhibited significantly higher radioactivity in xenografts than those of [^{125}I]SIB-NuB2 with no significant increase being observed in other tissues. The findings indicate that appropriate R_8 modification of antibodies satisfies both specific targeting ability of antibody and strong cell-association property of R_8, which was reflected in the increased radioactivity levels in tumor. These findings supported the applicability of this approach to enhance target-specific accumulation of radiolabeled antibodies.

INTRODUCTION

Radioimmunotherapy (RIT) is a cancer therapeutic modality that combines the specific tumor targeting of immunotherapeutics and cytotoxic radiation mechanisms. Encouraging results have been reported in patients with hematologic malignancies treated with ^{90}Y- and ^{131}I-labeled antibodies against CD20 (*1*−*4*), due to their intrinsic high radiosensitivity and relatively good access of the radiolabeled antibodies to the cancer cells (*5, 6*). Despite numerous efforts, the treatment of solid tumors with radiolabeled antibodies resulted in limited success, due to poor localization of radiolabeled antibodies in the tumors (*7*−*9*). Thus, the enhancement of tumor accumulation and retention of radiolabeled antibodies constitutes a prime requisite for successful RIT.

Numerous factors have been presented as being responsible for tumor accumulation and retention of radiolabeled antibodies (*8*). Since the mechanism of accumulation of radiolabeled antibodies is based on their specific but reversible binding to antigens in tumor tissues, a strategy that shifts the equilibrium to antigen association was considered of prime importance to enhancing tumor accumulation. The use of antibodies internalized to target cells would prolong residence time in the tumor, since these molecules will be resistant to being cleared by washout. The conjugation of arginine-rich cell-penetrating peptides (AR-CPPs) to antibodies has been conducted as a means to facilitate internalization of antibodies and to increase tumor accumulation. Indeed, a prior study reported an increase in tumor accumulation of AR-CPP-conjugated antibodies in vitro (*10*). However, in vivo studies showed increased accumulation in nontarget tissues such as the liver with decreased accumulation in tumors. A prior study also described that the tumor targeting ability of an antibody construct (scFv) was completely abolished following conjugation with AR-CPP (*11*).

Meanwhile, an increase in avidity of antibodies constitutes another strategy to enhance tumor accumulation, as observed in antibody constructs with multivalent binding domains (*8, 12, 13*). An increase in tumor uptake was also observed with divalent radiolabeled haptens in pretargeting strategy (*14*). These studies suggested that chemical modification of antibodies with anchoring molecules that possess strong interaction with cell surface molecules or cell membrane may also be useful to shift the equilibrium to antigen association in tumor tissues.

* Corresponding author. Yasushi Arano, Ph.D. Graduate School of Pharmaceutical Sciences, Chiba University, 1-8-1 Inohana, Chuo-ku, Chiba 260-8675, Japan. Phone: +81-43-226-2896; Fax: +81-43-226-2897; E-mail: arano@p.chiba-u.ac.jp.

[†] Chiba University.

[‡] Health Sciences University of Hokkaido.

[§] Kyoto University.

[∥] Gunma University.

[⊥] Suzuka University of Medical Science.

10.1021/bc100259q
Published on Web 10/25/2010

Scheme 1

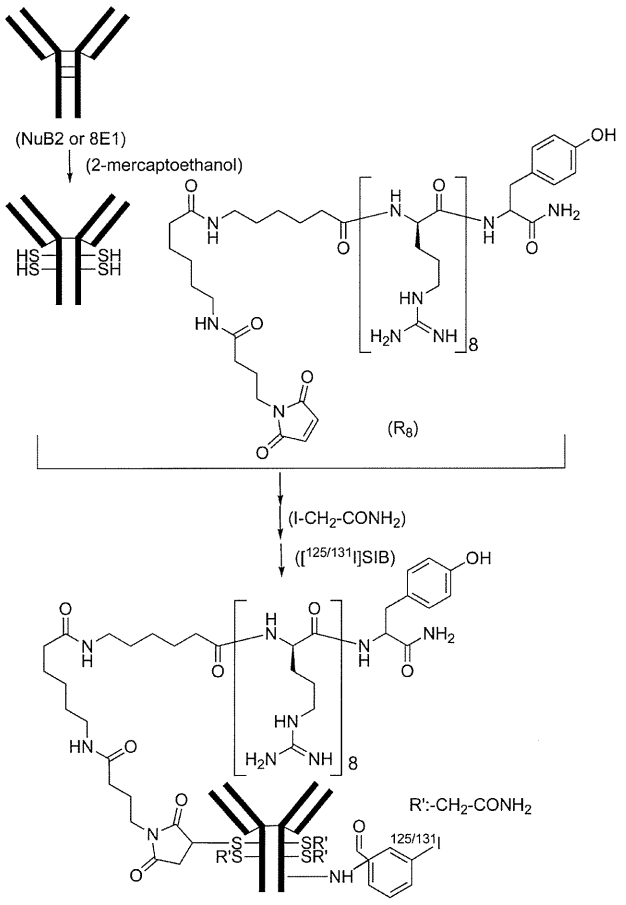

The AR-CPPs possess strong interaction with phosphate groups, sulfates, and carboxylates on cellular components (*15*−*18*). The electrostatic interaction between AR-CPPs and cell membrane is so strong that complete removal of AR-CPPs from the cell surface is difficult to perform (*19*−*21*). Such characteristics render AR-CPPs applicable as an anchoring molecule to shift the equilibrium to antigen association for prolonged retention of radiolabeled antibodies in tumors. In addition, the strong electrostatic interaction between AR-CPPs and cellular components suggested that AR-CPPs would exert their anchoring ability at conjugation levels much lower than those used for facilitating internalization.

In this study, an octaarginine peptide was selected as an anchoring molecule, and the peptide was derivatized with a maleimide group to conjugate with a relevant or irrelevant antibody against CD20 (Scheme 1). After radiolabeling of the modified antibodies with succinimidyl *meta*-[$^{125/131}$I]iodobenzoate ([$^{125/131}$I]SIB), the effect of the octaarginine conjugation on specific binding to target cells, dissociation rates from the cells, and biodistribution was determined with special emphasis being laid on the relationship between the anchoring ability of R_8 and the number of R_8 molecules attached per molecule of the antibody. The applicability of the new approach using an AR-CPP as an anchoring molecule to prolong residence time of radiolabeled antibodies in tumor will be discussed.

EXPERIMENTAL PROCEDURES

Reagents and Chemicals. Na[^{125}I]I and Na[^{131}I]I were obtained from MP Biomedicals (Irvine) and Perkin-Elmer (Yokohama, Japan), respectively. The stannyl precursor of the radioiodination reagents, *N*-succinimidyl-3-(tri-*n*-butylstannyl)-benzoate (ATE) was synthesized as reported previously (*22*). Size-exclusion high-performance liquid chromatography (SE-HPLC) was performed using a Cosmosil Diol-300 (7.5 × 600 mm, Nacalai Tesque, Kyoto, Japan) column at a flow rate of 1 mL/min with 0.1 M phosphate buffer (PB, pH 6.8) as an eluent. Each eluent was collected with a fraction collector (RediFlac, GE Healthcare Bioscience, Tokyo, Japan) at 1 min intervals. The radioactivity counts in each fraction (1 mL) were determined with an autowell γ counter (ARC-380M, Aloka, Tokyo). TLC analyses were performed with silica plates (Silica Gel 60 F_{254}, Merck, Tokyo). Isoelectric focusing (IEF) was conducted using a Tefco STC808 mini electrophoresis cell (Tefco, Tokyo) with a precast polyacrylamide gel isoelectric focusing (IEF-PAGE) mini isocratic gel (pH 3−10) (Tefco, Tokyo). Other reagents were of reagent grade and were used as received.

Cells and Antibodies. The CD20 positive human peripheral lymphocyte line RPMI 1788 cells were incubated with RPMI-1640 medium (Sigma-Aldrich Co, St. Louis, MO, USA) supplemented with 10% fetal calf serum and were used for the studies.

The monoclonal antibodies used in this study were a murine monoclonal antibody (NuB2; IgG2b) that reacts specifically with CD20 as a relevant antibody and a murine monoclonal antibody (8E1; IgG2a) specific to a neural protein as an irrelevant one, respectively, since both subclasses possess similar quaternary structures and the interchain disulfide bonds are the primary sites of chemical reduction for both antibodies (*23*). Both antibodies were kindly supplied from Immuno-Biological Laboratories Co, Ltd., (Takasaki, Japan).

Synthesis of Mal-(Acp)$_2$-(D-Arg)$_8$-(D-Tyr) (R_8). We employed D-octaarginine peptide as an AR-CPP, and the peptide with N-terminal bis-aminocaproate linker was coupled with *N*-(4-maleimidebutyryloxy)succinimide for antibody conjugation (Scheme 1).

The peptide chain of R_8 was constructed by Fmoc (9-fluorenylmethyloxycarbonyl) solid-phase peptide synthesis on a TGS-RAM resin (Shimadzu, Kyoto) using Shimadzu PSSM8 peptide synthesizer (Shimadzu, Kyoto) with its standard protocol. A 1-[bis(dimethylamino)methylene]-1*H*-benzotriazolium 3-oxide hexafluorophosphate/1-hydroxybenzotriazole/*N*,*N*-diisopropylethylamine coupling system was employed as the coupling system. As amino acid derivatives, Fmoc-Acp, Fmoc-D-Arg(Pdf), and Fmoc-D-Tyr(^{t}Bu) were used (Acp = 6-aminocaproic acid). The peptide resin was then treated with *N*-(4-maleimidobutyryloxy)succinimide (3 equiv) and *N*-methylmorpholine (3 equiv) in DMF at 37 °C for 20 min to yield a peptide resin bearing a maleimide moiety on its N-terminus. The final deprotection of the peptide resin using trifluoroacetic acid (TFA)−H_2O (95:5) at room temperature for 3 h followed by reverse-phase HPLC purification with a Cosmosil Protein-R (10 × 250 mm, Nacalai Tesque, Kyoto) at a flow rate of 1 mL/min with a gradient mobile phase starting from 14% A (H_2O containing 0.1% TFA) and 86% B (CH_3CN containing 0.1% TFA) to 44% A and 56% B in 15 min. The product was ascertained by matrix-assisted laser desorption ionization time-of-flight mass spectrometry (MALDI-TOFMS, Voyager-DE STR, Applied Biosystems, Tokyo). MALDI-TOFMS: 1822.14 [Calcd for $(M + H)^+$: 1822.16].

Preparation of R_8-Modified Antibodies. Two R_8-modified NuB2s with different R_8-conjugation levels ($NuB2_I$ and $NuB2_{III}$) were prepared by reducing the disulfide bonds of NuB2 as reported previously with some modifications (Scheme 1) (*22*). Briefly, NuB2 was concentrated in a nitrogen atmosphere to 6.0 mg/mL in well-degassed 0.1 M PB (pH 7.0) containing 2 mM EDTA. The antibody (1.0 mL) was allowed to react with 2-mercaptoethanol (2-ME, 1000 molar excess) by gently stirring at room temperature for 30 min. Excess 2-ME was then removed

by a centrifuged column procedure using Sephadex G-50 Fine (GE Healthcare, Tokyo) equilibrated and eluted with 0.1 M PB (pH 6.0) containing 2 mM EDTA. A small aliquot of the filtrate was sampled, and the number of exposed thiol groups was determined with 2,2-dipyridyl disulfide (*24*). The filtrate was then added to a reaction vial containing 1.5-fold R_8 (42.8 μL, 85.7 μg) for $NuB2_I$ or 5-fold R_8 for $NuB2_{III}$ in 0.1 M PB (pH 6.0). After the reaction mixture was agitated gently for 1.5 h at 25 °C, 500-fold molar excess of iodoacetamide (269 μL, 2.68 mg) in 0.1 M PB (pH 6.0) was added. The reaction mixture was further incubated for 30 min to alkylate the unreacted thiol groups. $NuB2_I$ and $NuB2_{III}$ were finally purified by the centrifuged column procedure, equilibrated, and eluted with PBS (0.01 M, pH 7.4; Wako, Tokyo). Both $8E1_I$ and $8E1_{III}$ were prepared according to the procedure described above except for using 8E1 in place of NuB2.

Preparation of [$^{125/131}$I] *N*-Succinimidyl 3-Iodobenzoate (SIB)-Labeled Antibodies. *N*-Succinimidyl 3-(tri-*n*-butylstannyl)benzoate (ATE) was synthesized and radio-iodinated in the presence of *N*-chlorosuccinimide (NCS) as described previously (*25*). Briefly, ATE was dissolved in methanol containing 1% acetic acid (0.45 mg/mL), and 16.2 μL of this solution was mixed with 4.4 μL of NCS in methanol (0.5 mg/mL) in a sealed vial, followed by addition of Na[^{125}I]I (2 μL). After incubation at room temperature for 45 min, the reaction was quenched with aqueous sodium bisulfite (2.2 μL, 0.72 mg/mL). The radiochemical yield of [^{125}I]SIB was determined by TLC developed with ethyl acetate. The solvent was removed under a stream of N_2 prior to subsequent conjugation reaction with the antibodies. Conjugation of [^{125}I]SIB with antibodies was performed according to our previous procedure (*22*), with slight modifications as follows: A solution of $NuB2_I$, $NuB2_{III}$, $8E1_I$, or $8E1_{III}$ (120 μL, 2.5 mg/mL) in 0.2 M borate buffer (pH 8.5) was added to the dried residue of crude [^{125}I]SIB. After gentle incubation for 1 h at room temperature, [^{125}I]SIB-labeled antibodies were purified by the centrifuged column procedure, equilibrated, and eluted with PBS. Radioiodination of ATE with Na[^{131}I]I was performed as described above except for using Na[^{125}I]I in place of Na[^{131}I]I. Radiochemical purities of radiolabeled antibodies were also determined by SE-HPLC and TLC developed with 80% methanol/H_2O.

Preparation of ^{125}I-NuB2. Direct radioiodination of NuB2 was performed by the chloramine T method (*22*). To a solution of NuB2 (0.25 mg/mL; 200 μL) in 0.3 M PB (pH 7.5) was added 5 μL of Na[^{125}I]I. Chloramine T (0.1 mg/mL, 25 μL), freshly prepared in the same buffer, was then added. After incubation of the mixture for 10 min at room temperature, the reaction was terminated by an addition of 6 μL of aqueous sodium bisulfite (0.7 mg/mL). ^{125}I-NuB2 was purified by the centrifuged column procedure. The radiochemical purity was determined by SE-HPLC and TLC developed with 80% methanol/H_2O.

Preparation of Fluoresced Antibodies. NuB2, $NuB2_I$, and $NuB2_{III}$ were also labeled with Alexa Fluor 488 (AF, Molecular Probes, Tokyo). The fluorophore was dissolved in dimethylformamide at a concentration of 10 mg/mL, and the conjugation reaction was performed with a 5-fold molar excess of the fluorophore in 0.1 M sodium carbonate−sodium bicarbonate buffer (pH 9.0). After 1 h at room temperature, the reaction was terminated by an addition of freshly prepared 1.5 M hydroxylamine, and the fluorescent antibodies were purified by the centrifuged column procedure. The protein concentration in the purified conjugates was determined spectrophotometrically by subtracting 0.11 $A_{495\ nm}$ of the fluorophore from the $A_{280\ nm}$ of the antibody. The degree of labeling was calculated by dividing the $A_{495\ nm}$ of the fluorophore by the molar concentration of the antibodies and the dye extinction coefficient of 71 000 M^{-1} cm^{-1}.

Immunoreactivity. The immunoreactivity of radiolabeled NuB2s was assessed by the competitive immunoassay (*26*). To minimize nonspecific binding of radioiodinated antibodies to plastic tubes, the tubes were presaturated with a freshly prepared solution of 1% bovine serum albumin in PBS for 30 min, followed by three washes with PBS (*27*). Nonradioactive SIB-NuB2, SIB-$NuB2_I$, and SIB-$NuB2_{III}$ were prepared by experimental procedures similar to those used for [^{125}I]SIB-labeled antibodies, except that nonradioactive NaI was used in place of Na[^{125}I]I. A mixed solution of 50 μL ^{125}I-NuB2 and 50 μL nonradioactive SIB-NuB2, SIB-$NuB2_I$ or SIB-$NuB2_{III}$ (0.05−10 μg) was incubated in the presence of 1×10^6 RPMI 1788 cells suspended in 100 μL of PBS at 37 °C for 1 h. After centrifugation at 10 000 × *g* for 5 min, supernatant was discarded and the cell-associated radioactivity was determined using an auto γ counter.

RPMI 1788 Cell Binding and Retention. The cell binding of [^{125}I]SIB-labeled antibodies was also evaluated according to the procedure of Foulon et al. with slight modification (*28*). Approximately 1 μg each of [^{125}I]SIB-labeled antibodies was incubated with 1×10^6 RPMI 1788 cells for 1 h at 37 °C. Aliquots of cells in triplicate were removed, centrifuged, and washed with cold media. Then, the cell-associated radioactivity was determined as described above. Similar studies were conducted in the presence of 1000-fold excess of unlabeled NuB2.

The rest of the cells were resuspended in RPMI 1640 media containing 10% fetal bovine serum and 20 mM HEPES to a density of 3×10^6 cells/mL. After incubation for 1 and 3 h, aliquots of cells in triplicate were removed, centrifuged, and washed twice with cold media, and the cell-associated radioactivity was determined.

Confocal Microscopy. For each assay, 6×10^6 cells were plated into 35 mm glass-bottomed dishes. The cells were then incubated at 37 °C for 1 h with a fresh solution of NuB2, $NuB2_I$, or $NuB2_{III}$ (60 μL, 0.1 mg/mL) in cold RPMI 1640 media containing 10% FCS and 20 mM HEPES. The cells were washed twice with the same medium at 4 °C. The acidotropic dye LysoTracker Red DND-99 (Molecular Probes, Eugene, OR) was diluted in DMSO. The cells were resuspended in prewarmed (37 °C) medium containing 50 nM LysoTracker Red for 30 min. For live-cell imaging, aliquots of cells in 35 mm glass-based dishes were analyzed by confocal microscopy using a Fluoview FV500 (Olympus, Tokyo). Images were obtained at low-power laser (0.3−3.0% laser) using the 488 nm line of an argon laser. All images were obtained as 10 μm thicknesses of one planar (*xy*) section. The cells were maintained at 37 °C in a temperature-controlled box.

In Vivo Studies. Animal studies were conducted in accordance with our institutional guidelines and were approved by Chiba University Animal Care Committee. Biodistribution studies were performed by intravenous administration of a PBS solution of [^{125}I]SIB-NuB2, [^{125}I]SIB-$NuB2_I$, or [^{125}I]SIB-$NuB2_{III}$ to 6-week-old male ddY mice (Japan SLC Inc., Shizuoka, Japan). Groups of five mice, each receiving 0.3 μCi (20 μg/100 μL) of the antibodies, were used for the experiments. Organs of interest were removed and weighed, and the radioactivity counts were determined with an autowell γ counter at 1, 3, and 24 h postinjection.

Severe combined immunodeficiency (SCID) mice (C.B-17/IcrCrj-scid, Charles River Japan, Kanagawa, Japan) bearing xenograft of RPMI 1788 cells were also treated with a mixed solution of [^{131}I]SIB-$NuB2_I$ and [^{125}I]SIB-NuB2. The biodistribution of radioactivity after i.v. administration of the mixture

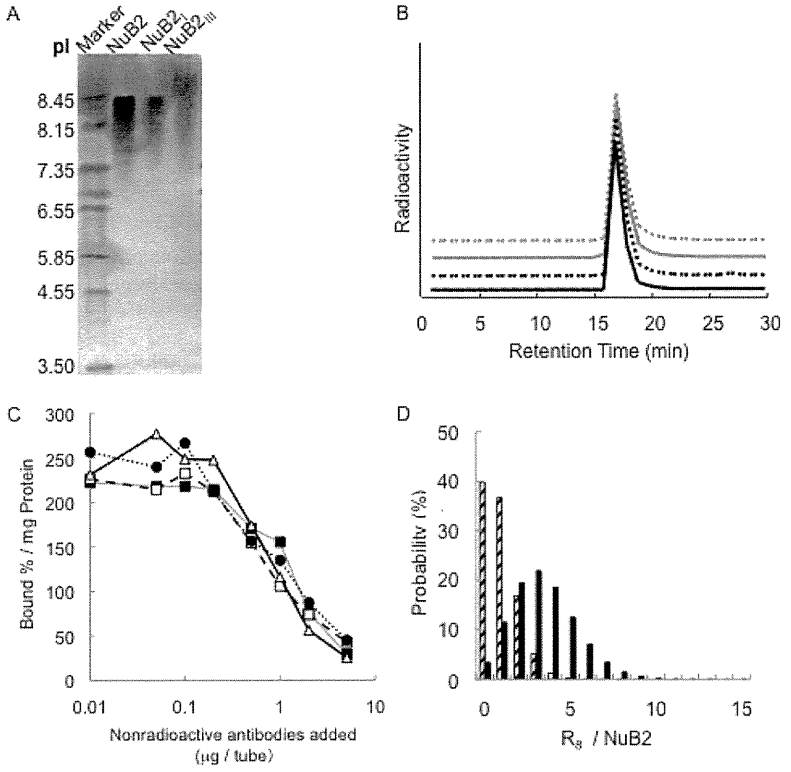

Figure 1. Characterization of R_8-conjugated antibodies ($NuB2_I$ and $NuB2_{III}$). (A) Isoelectric focusing. While both NuB2 and $NuB2_I$ showed similar profiles, a wider band toward higher pI was observed with $NuB2_{III}$. (B) Size-exclusion HPLC profiles. ^{125}I-NuB2: black solid line. [^{125}I]SIB-NuB2: black broken line. [^{125}I]SIB-$NuB2_I$: gray solid line. [^{125}I]SIB-$NuB2_{III}$: gray broken line. All the radioiodinated NuB2s exhibited similar elution profiles. (C) Competitive immunoassay to RPMI 1788 cells. Increasing concentrations of nonradioactive iodine-labeled NuB2s (NuB2 (solid square), SIB-NuB2 (square), SIB-$NuB2_I$ (circle), SIB-$NuB2_{III}$ (triangle)) and 1×10^6 RPMI 1788 cells were incubated in the presence of [^{125}I]-labeled NuB2. No significant differences were observed among the four NuB2s. (D) Poisson distribution profiles of $NuB2_I$ (hatched column) and $NuB2_{III}$ (solid column).

to 8-week-old SCID mice was monitored at 24, 48, 72, and 96 h postinjection. Groups of 5−7 mice, each receiving 0.3 μCi (10 μg each) of antibodies, were used for the experiments. Organs of interest were removed and weighed, and the radioactivity counts were determined with an autowell γ counter. A window from 29 to 97 keV was used for counting ^{125}I, whereas one from 280 to 440 keV was used for ^{131}I. Correlation factors to eliminate crossover of ^{131}I activity into ^{125}I were determined by counting ^{131}I standard in each window. The crossover of ^{125}I into the ^{131}I channel was negligible.

Statistical Analysis. Data are expressed as means ± standard deviation where appropriate. Results were statistically analyzed with an unpaired Student's *t*-test using the Microsoft *Excel* program. Differences were considered statistically significant when the *p* value was less than 0.05.

RESULTS

Preparation of Conjugates. Conjugation of NuB2 or 8E1 with R_8 was performed by maleimide−thiol chemistry using thiol groups generated by reducing the disulfide bonds of the antibody molecule. The numbers of R_8 molecule attached per molecule of NuB2 were determined to be 0.92 for $NuB2_I$ and 3.38 for $NuB2_{III}$. Similar procedures were employed for the preparation of $8E1_I$ and $8E1_{III}$ where the number of R_8 per molecule of 8E1 was estimated to be 0.98 and 3.85, respectively. The pI values of NuB2, $NuB2_I$, and $NuB2_{III}$ were determined by the isoelectric focusing and found to be 7.5−8.6, 7.5−8.6, and 7.5−9.0, respectively (Figure 1A). All [$^{125/131}$I]SIB-labeled antibodies had radiochemical purities over 95% when determined by the SE-HPLC (Figure 1B) and TLC. ^{125}I-NuB2 was prepared by the chloramine T method with radiochemical purity of 99%. AF-NuB2, AF-$NuB2_I$, and AF-$NuB2_{III}$ were labeled with Alexa Fluor 488 with a conjugation level of 3.67, 3.89, and 3.57 molecules of the fluorophore per molecule of each antibody.

Immunoreactivity Measurement. Figure 1C shows the RPMI 1788 cell binding of ^{125}I-NuB2 in the presence of unlabeled NuB2, nonradioactive SIB-conjugated NuB2, SIB-$NuB2_I$, and SIB-$NuB2_{III}$. Unlabeled NuB2 almost completely inhibited the binding of ^{125}I-NuB2 to RPMI 1788 cells, and no significant differences were observed in the inhibitory curves among the nonradioactive SIB-NuB2, SIB-$NuB2_I$, and SIB-$NuB2_{III}$. Similar results were observed with AF-labeled antibodies (data not shown).

Localization of the Antibodies in RPMI 1788 Cells. Figure 2A shows the localization of NuB2, $NuB2_I$, and $NuB2_{III}$ in living cells when determined by confocal microscopy. All AF-labeled antibodies (green) were present on the cell membrane. Under the conditions, LysoTracker (red) was observed in acidic compartment of the cells such as endosome and lysosome.

In Vitro Cell Binding and Retention. When the radiolabeled antibodies were incubated with the RPMI 1788 cell at 1 h at 37 °C, [^{125}I]SIB-$NuB2_I$ and [^{125}I]SIB-$NuB2_{III}$ showed 1.4 and 4.3 times higher cell-associated radioactivity than [^{125}I]SIB-NuB2 (Figure 2B). When the radiolabeled antibodies were incubated in the presence of 1000-fold excess of NuB2, significant reduction in the cell-associated radioactivity was observed with [^{125}I]SIB-NuB2 and [^{125}I]SIB-$NuB2_I$. However, [^{125}I]SIB-$NuB2_{III}$ still registered high cell-associated radioactivity. Similarly, higher cell-associated radioactivity was observed

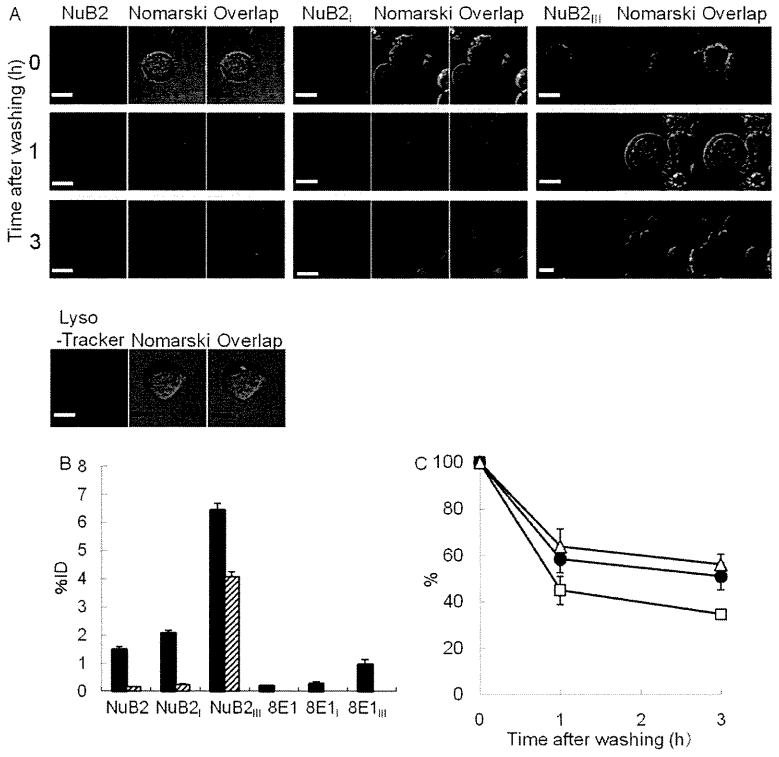

Figure 2. Cellular processing of [^{125}I]SIB-NuB2s. (A) Confocal microscopy to detect NuB2s localization (green) in RPMI 1788 cells as a function of incubation intervals at 37 °C; bars, 10 μm. (B) RPMI 1788 cell-associated radioactivity after 1 h incubation of [^{125}I]SIB-NuB2s at 37 °C (solid column). Similar experiments were performed in the presence of 1000-fold excess of NuB2 (hatched column). (C) Retention of [^{125}I]SIB-labeled NuB2s ([^{125}I]SIB-NuB2 (square), [^{125}I]SIB-NuB2$_{I}$ (solid circle), [^{125}I]SIB-NuB2$_{III}$ (triangle)) on RPMI 1788 cells after washing and reincubation in a fresh medium for 1 and 3 h (average of triplicates and SD).

in [^{125}I]SIB-8E1$_{III}$ when compared with [^{125}I]SIB-8E1 and [^{125}I]SIB-8E1$_{I}$.

Figure 2C shows the retention of [^{125}I]SIB-NuB2, [^{125}I]SIB-Nub2$_{I}$, and [^{125}I]SIB-NuB2$_{III}$ from RPMI 1788 cells as a function of reincubation times. While [^{125}I]SIB-NuB2 showed 44.3% and 34.2% of the initial radioactivity levels at 1 and 3 h postincubation, [^{125}I]SIB-NuB2$_{I}$ exhibited the cell-bound radioactivity of 59.1% and 51.2% at the same postincubation times. [^{125}I]SIB-NuB2$_{III}$ showed radioactivity levels of 67.8% and 61.3% at 1 and 3 h postincubation, respectively.

In Vivo Studies. The biodistribution of radioactivity after intravenous injection of [^{125}I]SIB-NuB2, [^{125}I]SIB-NuB2$_{I}$, and [^{125}I]SIB-NuB2$_{III}$ to normal mice is summarized in Table 1. Both [^{125}I]SIB-NuB2 and [^{125}I]SIB-NuB2$_{I}$ showed similar radioactivity levels in the blood, liver, kidney, and intestine. However, [^{125}I]SIB-NuB2$_{III}$ exhibited faster clearance of the radioactivity from the blood with higher radioactivity levels in the liver throughout the postinjection time examined. As a result, [^{125}I]SIB-NuB2$_{III}$ exhibited higher liver-to-blood ratios of the radioactivity.

Table 2 shows the biodistribution of the radioactivity after simultaneous injection of [^{125}I]SIB-NuB2 and [^{131}I]SIB-NuB2$_{I}$ in SCID mice bearing RPMI 1788 cells. [^{131}I]SIB-NuB2$_{I}$ exhibited significantly higher radioactivity levels in the tumor than those observed with [^{125}I]SIB-NuB2 from 48 to 96 h postinjection. [^{131}I]SIB-NuB2$_{I}$ exhibited similar radioactivity levels in other tissues such as the blood, liver, kidney, and intestine when compared with [^{125}I]SIB-NuB2.

Table 1. Biodistribution of Radioactivity after Intravenous Injection of [^{125}I]SIB-NuB2, [^{125}I]SIB-NuB2$_{I}$, and [^{125}I]SIB-NuB2$_{III}$ in Normal Mice[a]

	time after injection		
	1 h	3 h	24 h
	[^{125}I]SIB-NuB2		
blood	26.51 (0.99)	22.37 (1.33)	12.63 (0.48)
liver	7.65 (0.49)	5.99 (0.34)	3.34 (0.29)
kidney	5.92 (0.43)	5.46 (1.68)	3.31 (0.15)
stomach[b]	0.56 (0.55)	0.84 (0.08)	1.27 (0.44)
intestine	1.30 (0.07)	1.69 (0.15)	1.36 (0.33)
liver/blood	0.29 (0.03)	0.27 (0.00)	0.26 (0.01)
	[^{125}I]SIB-NuB2$_{I}$		
blood	26.26 (0.83)	20.70 (0.14)	10.54** (0.61)
liver	7.03 (0.3)	5.72 (0.33)	2.81 (0.40)
kidney	6.85* (0.31)	5.38 (0.50)	3.37 (0.35)
stomach[b]	0.58 (0.06)	1.01* (0.07)	1.89 (0.95)
intestine	1.15 (0.17)	1.68 (0.04)	0.95 (0.16)
liver/blood	0.27 (0.01)	0.28 (0.02)	0.27 (0.03)
	[^{125}I]SIB-NuB2$_{III}$		
blood	20.32 (3.79)	15.45** (1.36)	8.08** (0.49)
liver	17.91** (0.42)	14.71** (0.46)	5.85** (0.69)
kidney	6.50 (0.73)	5.80 (0.57)	3.42 (0.17)
stomach[b]	0.86** (0.05)	1.30* (0.25)	1.66 (0.67)
intestine	1.01 (0.08)	1.42 (0.30)	0.82 (0.17)
liver/blood	0.90** (0.14)	0.96** (0.12)	0.72** (0.05)

[a] Tissue radioactivity is expressed as percent of injected dose per gram of wet tissue. Results are expressed as means (SD) of three animals each point. [b] Expressed as percent of injected dose per tissue. Significances determined by unpaired Student's *t*-test. * $p < 0.05$ compared to [^{125}I]SIB-NuB2. ** $p < 0.01$ compared to [^{125}I]SIB-NuB2.

DISCUSSION

In this study, we estimate the ability of an octaarginine peptide, R_8, as an anchoring molecule to enhance target accumulation of radiolabeled antibodies. The spatial location of the anchoring molecules attached to an antibody was considered of importance to maintain antigen binding properties, specific binding, and biodistribution profiles of the parental